UC Berkeley

UC Berkeley Previously Published Works

Title

Engineered Biosynthesis of Alkyne-Tagged Polyketides by Type I PKSs

Permalink

https://escholarship.org/uc/item/2xp6c39k

Journal

iScience, 23(3)

ISSN

2589-0042

Authors

Porterfield, William B
Poenateetai, Nannalin
Zhang, Wenjun

Publication Date

2020-03-01

DOI

10.1016/j.isci.2020.100938

Peer reviewed

eScholarship.org Powered by the California Digital Library
University of California

iScience

CellPress

Article

Engineered Biosynthesis of Alkyne-Tagged Polyketides by Type I PKSs

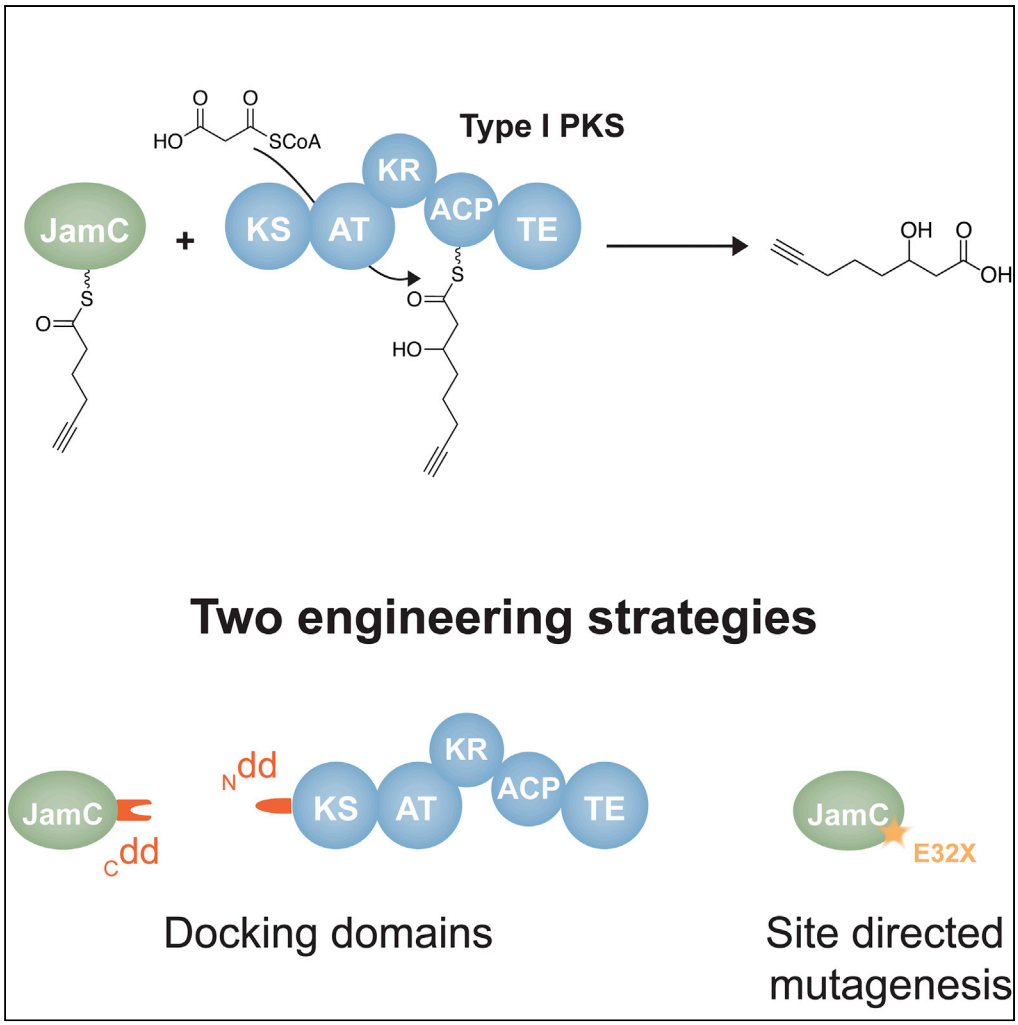

William B. Porterfield, Nannalin Poenateetai, Wenjun Zhang

wjzhang@berkeley.edu

HIGHLIGHTS

Alkyne-tagged polyketides are *de novo* biosynthesized using type I PKSs

Docking domains and ACP mutagenesis improve alkyne starter unit translocation

Docking domains, but not ACP mutagenesis, perturb alkyne biosynthetic machinery

Porterfield et al., iScience *23*, 100938
March 27, 2020 © 2020 The Author(s).
https://doi.org/10.1016/j.isci.2020.100938

iScience

CellPress

Article

Engineered Biosynthesis of Alkyne-Tagged Polyketides by Type I PKSs

William B. Porterfield,[1] Nannalin Poenateetai,[1] and Wenjun Zhang[1,2,3,*]

SUMMARY

Polyketides produced by modular polyketide synthases (PKSs) are important small molecules widely used as drugs, pesticides, and biological probes. Tagging these polyketides with a clickable functionality enables the visualization, diversification, and mode of action study through bio-orthogonal chemistry. We report the *de novo* biosynthesis of alkyne-tagged polyketides by modular type I PKSs through starter unit engineering. Specifically, we use JamABC, a terminal alkyne biosynthetic machinery from the jamaicamide B biosynthetic pathway, in combination with representative modular PKSs. We demonstrate that JamABC works as a *trans* loading system for engineered type I PKSs to produce alkyne-tagged polyketides. In addition, the production efficiency can be improved by enhancing the interactions between the carrier protein (JamC) and PKSs using docking domains and site-directed mutagenesis of JamC. This work thus provides engineering guidelines and strategies that are applicable to additional modular type I PKSs to produce targeted alkyne-tagged metabolites for chemical and biological applications.

INTRODUCTION

Natural products produced by modular polyketide synthases (PKSs) have demonstrated their use as therapeutics, industrial products, pesticides, and biological probes following intense study over the past decades (Hertweck, 2009; Klaus and Grininger, 2018). Some well-known examples of these polyketides include the antibiotic erythromycin and the immunosuppressant rapamycin, both of which were initially isolated from bacterial sources and have been approved for clinical use for decades (Cottens et al., 2019; Hertweck, 2009; Jelic and Antolovic, 2016). The process for discovery, diversification, and mode of action elucidation of polyketides remains challenging and time consuming, although it has been improved in recent years due to many technical advancements. One such technology is to tag polyketides with a clickable functionality, which has been demonstrated to facilitate the study of polyketide biosynthesis, biology, and pharmacology through bio-orthogonal chemistry (DeGuire et al., 2015; Harvey et al., 2012; Hughes et al., 2014; Kalkreuter et al., 2019a, 2019b; Koryakina et al., 2017; Musiol-Kroll et al., 2017; Riva et al., 2014; Seidel et al., 2019; Zhu and Zhang, 2015). In particular, polyketides can be tagged through semi-synthesis (DeGuire et al., 2015; Seidel et al., 2019), total synthesis (Staub and Sieber, 2008), precursor-directed biosynthesis (Harvey et al., 2012; Koryakina et al., 2017; Musiol-Kroll et al., 2017; Seidel et al., 2017; Yan et al., 2013), or *de novo* biosynthesis (Zhu et al., 2015a; Zhu and Zhang, 2015). In this work we aim to further develop the strategy of *de novo* biosynthesis, which offers the unique advantage of not feeding the biorthogonal moiety itself, which could lead to increased background due to the diffusible non-specific nature of feeding starter or extender units. Instead the taggable group is incorporated by enzymatically synthesizing both the complex polyketide scaffolds and the unique clickable functionality allowing *in situ* bio-orthogonal chemical transformations.

Modular PKSs, often referred to as type I PKSs, have modules with multiple catalytic domains that perform separate enzymatic activities and act as an assembly line to select and incorporate building monomers into polyketide scaffolds (Jenke-Kodama and Dittmann, 2009; Keatinge-Clay, 2012; Khosla et al., 2014; Ladner and Williams, 2016) (Figure 1). The monomers used for extension, typically malonyl- or methylmalonyl-CoA, are recognized by acyltransferase (AT) domains, and the carbon-carbon bond is formed through decarboxylative Claisen condensations catalyzed by the ketosynthase (KS) domains. The megasynthases themselves have been investigated and have undergone extensive engineering efforts due to their modular structures that have captured scientists' imagination with the possibility of producing on-demand, designer molecules (Awakawa et al., 2018; Barajas et al., 2017; Chemler et al., 2015; Harvey et al., 2012; Kalkreuter and Williams, 2018; Klaus and Grininger, 2018; Koryakina et al., 2017; Moss et al., 2013; Ranganathan et al., 1999; Sundermann et al., 2013; Tang et al., 2000; Wlodek et al., 2017; Yonemoto et al., 2012; Yuzawa

[1]Department of Chemical and Biomolecular Engineering, University of California, Berkeley, CA 94709, USA

[2]Chan Zuckerberg Biohub, San Francisco, CA 94158, USA

[3]Lead Contact

*Correspondence: wjzhang@berkeley.edu

https://doi.org/10.1016/j.isci.2020.100938

This is an open access article under the CC BY-NC-ND license (http://creativecommons.org/licenses/by-nc-nd/4.0/).

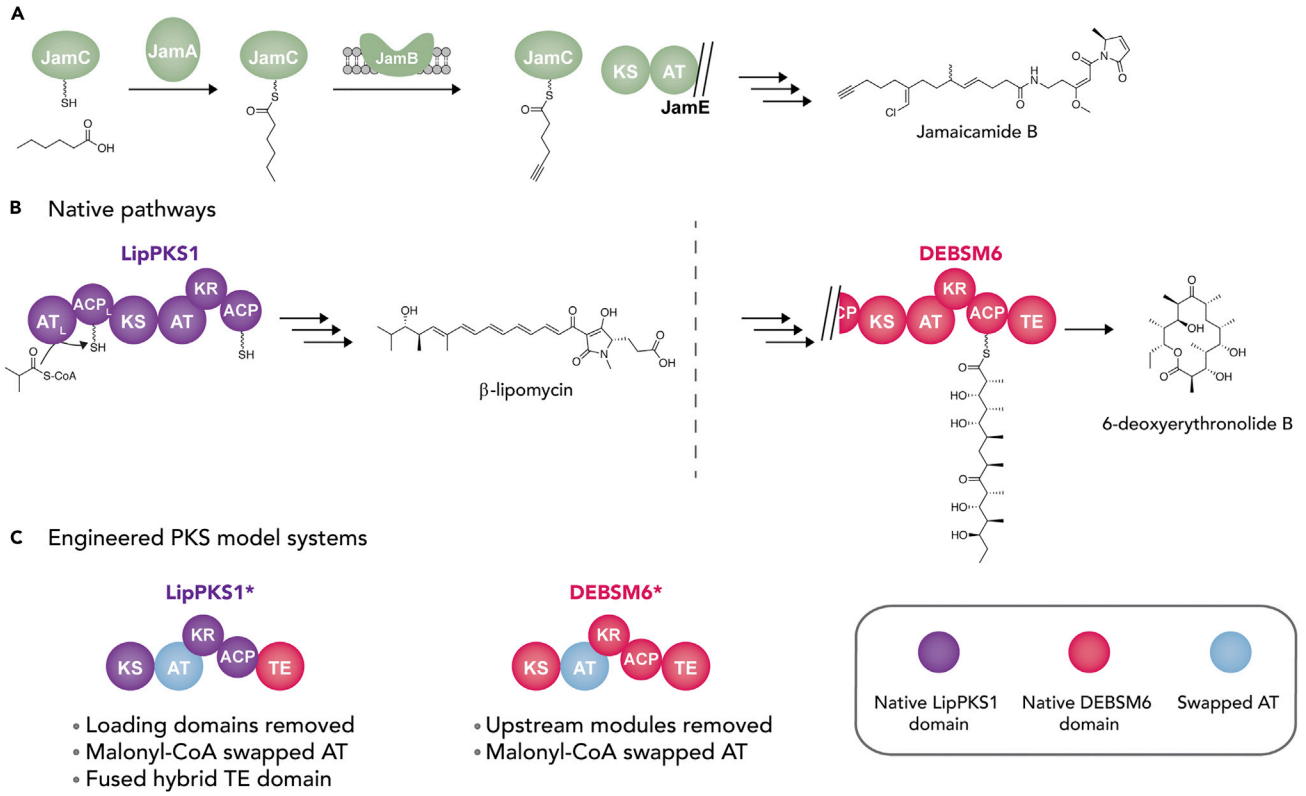

Figure 1. Overview of the JamABC Cassette and Type I PKSs in This Work

(A) JamABC works together to produce 5-hexynoyl-JamC as a starter unit for the downstream PKS/nonribosomal peptide synthetase assembly line in jamaicamide B biosynthesis.

(B) Native LipPKS1 and DEBSM6 domain organization and associated polyketide products.

(C) Engineered LipPKS1* and DEBSM6* used as representative modular PKSs in the current study.

et al., 2017). Many of these engineering strategies have included efforts geared toward the inclusion of functional chemical handles for subsequent drug discovery or chemical biology studies, albeit often employing fed precursors containing the functionality of interest (Kalkreuter et al., 2019a; Koryakina et al., 2017; Mohammadi-Ostad-Kalayeh et al., 2018).

The terminal alkyne is a canonical bio-orthogonal functional group as it is small, stable, and can be selectively reacted via copper-catalyzed azide-alkyne cycloaddition, where an azide containing a fluorophore, mass tag, or other chemical moiety is attached (Prescher and Bertozzi, 2005; Zhu and Zhang, 2015). The bio-orthogonality of alkynes is due to its chemical stability in biological environments and its rarity in biology where only a small number of terminal alkyne-bearing secondary metabolites have been discovered and even fewer biosynthetic pathways have been elucidated (Edwards et al., 2004; Fritsche et al., 2014; Haritos et al., 2012; Lee et al., 1998; Marchand et al., 2019; McPhail et al., 2007; Minto and Blacklock, 2008; Moss et al., 2019; Ross et al., 2014). We recently identified and characterized an acyl carrier protein (ACP)-dependent, three-protein pathway to generate the terminal alkyne functionality in *E. coli* (Zhu et al., 2015a, 2015b, 2016). For example, in the biosynthesis of the cyanobacterial jamaicamide B, JamA, an acyl-ACP synthetase, activates and loads 5-hexanoic acid onto JamC, a dedicated ACP. The resulting 5-hexanoyl-JamC is modified by JamB, a membrane-bound desaturase/acetylenase, to yield 5-hexynoyl-JamC as a starter unit for the downstream PKS/nonribosomal peptide synthetase assembly line (Figure 1A) (Edwards et al., 2004; Zhu et al., 2015a). *JamABC* thus represents a portable tri-gene cassette that may be useful for *in situ* generation and incorporation of terminal alkynes into various molecular scaffolds on demand. Toward this end, we demonstrated that PKS starter unit engineering is a feasible strategy to install the fatty alkynyl starter unit generated by JamABC onto polyketide scaffolds, such as those generated by promiscuous type III PKSs, which recognize both the acyl group and the acyl carrier (JamC) (Zhu et al., 2015a, 2015b). However,

to generalize this strategy to other polyketide scaffolds, in particular those synthesized by modular type I PKSs, additional model systems and protein engineering methods need to be explored.

Here we employ two well-studied type I PKSs, LipPKS1 and DEBSM6, to explore engineering strategies to make alkyne-tagged polyketides. LipPKS1 is the first module in lipomycin biosynthesis that natively utilizes an isobutyl starter unit presented by a loading ACP (Figure 1B) (Bihlmaier et al., 2006). DEBSM6 is the last PKS module from the erythromycin biosynthetic pathway (Figure 1B) (Rawlings, 2001). In addition, engineered LipPKS1 and DEBSM6 have been obtained to utilize malonyl-CoA instead of methylmalonyl-CoA as the extender unit with the promiscuous DEBS thioesterase to promote the acid product release as demonstrated from both *in vitro* biochemical studies and in *E. coli* (Yuzawa et al., 2017). These two engineered modules are thus simple and convenient systems for in-depth assessment of the interaction between representative module PKSs and JamABC for alkyne-tagged polyketide biosynthesis. Considering the known critical role of the cognate ACP (JamC) in the alkyne biosynthetic machinery (Su et al., 2018; Zhu et al., 2015a), the recognition of JamC by PKSs is expected to play a key role in alkyne-tagged polyketide synthesis and therefore is the focus of the present study.

RESULTS AND DISCUSSION

Alkyne-Tagged Polyketide Synthesis *In Vitro*

To probe the possible recognition of the 5-hexynoyl-JamC by PKSs, *in vitro* assays were initially performed using the engineered LipPKS1 and DEBSM6 modules. The reported engineered LipPKS1 was further modified by removing the AT and ACP loading domains to create a truncated version to facilitate the alternative starter unit incorporation. We hypothesized that these engineered PKSs (termed LipPKS1* and DEBSM6*, Figure 1C) without the loading domains would result in JamC to act in *trans* to selectively load and extend JamC-linked acyl chains. For *in vitro* assessment we purified JamA, holo-JamC, and LipPKS1*/DEBSM6* from *E. coli* after overexpression (Figure S1), or an *E. coli* BAP1 strain that contains a chromosomal copy of the phosphopantetheinyl transferase Sfp that was used to ensure the post-translational modification of carrier proteins to the pantetheinylated forms (Pfeifer et al., 2001). Purified enzymes were incubated with 5-hexynoic acid, ATP, malonyl-CoA, and NADPH for alkyne-tagged polyketide biosynthesis *in vitro* (Figure 2A). JamB activity for alkyne biosynthesis was not assessed *in vitro* due to the difficulty of obtaining active and purified membrane proteins and was assessed later *in vivo*. The expected product, 3-hydroxy-7-octynoic acid (**1**), was successfully produced by both engineered PKSs as confirmed by comparing with the synthetic chemical standard (Figures 2B, 2C, and S2–S4, Scheme S1). Interestingly, replacement of 5-hexynoyl-JamC by 5-hexynoyl-CoA, which was generated *in situ* using a promiscuous acyl-CoA ligase Orf35 (Zhang et al., 2010), dropped the formation of **1** to trace amounts, demonstrating a preference of these two PKSs toward JamC over CoA as the acyl carrier (Figures 2B, 2C, and S2).

Evaluation of Docking Domain Strategy to Improve JamC-PKS Interactions

As protein-protein interactions are known to dominate the turnover of chimeric PKS assembly lines (Klaus et al., 2016), we proposed that improved communication between the upstream JamC and the downstream KS could lead to a more efficient alkyne-tagged polyketide biosynthesis. Docking domains, often found on the C terminus of ACPs (dd^{ACP}) and the N terminus of KSs (dd^{KS}), have been shown to be important for protein-protein interactions in PKSs (Gokhale et al., 1999; Tsuji et al., 2001; Zeng et al., 2016). We then set out to evaluate the strategy of fusing known docking domains to the C terminus of JamC and the N terminus of the LipPKS1*/DEBSM6* KS domains to improve protein recognition. In particular, we chose to utilize the class 2 docking domains from the cyanobacterial curacin pathway as the pair $_{C}dd^{CurK}$ (dd^{ACP}) and $_{N}dd^{CurL}$(dd^{KS}) was shown to be modular and portable (Whicher et al., 2013). We also chose the related docking domain pair $_{C}dd^{JamK}$ (dd^{ACP}) and $_{N}dd^{JamL}$(dd^{KS}) from the jamaicamide pathway as moving docking domains within pathways was shown to be more successful than inter-pathway swapping (Klaus and Grininger, 2018; Klaus et al., 2016; Whicher et al., 2013). The fusion of these docking domains to JamC and PKSs did not significantly impact the expression and folding of these proteins (Figures S1 and S5). *In vitro* product formation assays using purified proteins demonstrated the success of this strategy in generating product **1** (Figures 2 and S6). The adoption of the pair of $_{C}dd^{JamK}$ and $_{N}dd^{JamL}$ had minimal effect on the production of **1**, whereas the pair of $_{C}dd^{CurK}$ and $_{N}dd^{CurL}$ led to significantly more amount of **1** in both PKS systems (~3-fold for LipPKS1* and ~40-fold for DEBSM6*) (Figures 2B and 2C). Control experiments using only one of the docking domains produced less products than using the pair for $_{C}dd^{CurK}$ and $_{N}dd^{CurL}$. In addition, the poor production of **1** with the docking domain fused to JamC excluded the possibility of improved recognition of modified JamC by JamA (Figures 2B and 2C), indicating that the

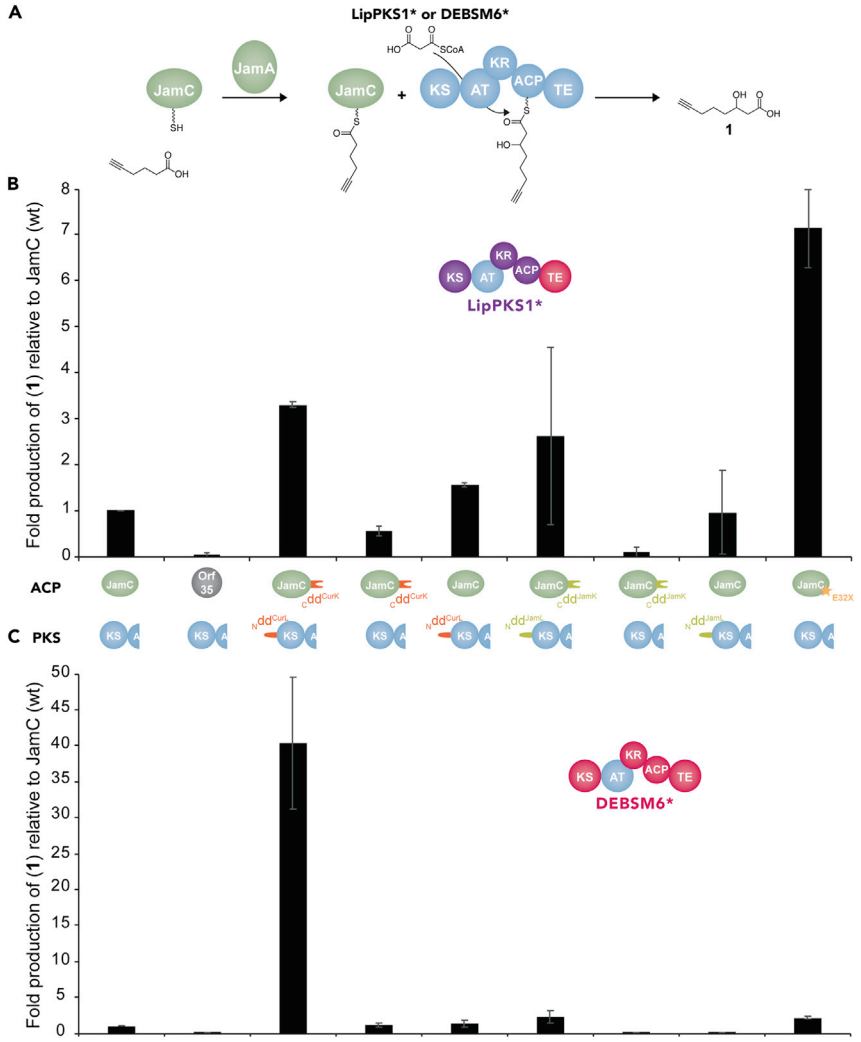

Figure 2. *In Vitro* Assessment of Alkyne-Tagged Polyketide Biosynthesis Using LipPKS1* and DEBSM6*

(A) Overview scheme of *in vitro* reactions between JamA/JamC and engineered PKSs to produce 3-hydroxy-7-octynoic acid (**1**).

(B) Formation of **1** by LipPKS1* under various reaction conditions and engineering strategies.

(C) Formation of **1** by DEBSM6* under various reaction conditions and engineering strategies. Engineered PKS cartoon is truncated for clarity. All graphs are shown as relative product formed compared with the JamC/PKS with no modifications calculated from integration of the extracted ion chromatogram (EIC) for compound **1** (set as 1). Error bars indicate SEM for n ≥ 2 independent experiments.

improved communication between the engineered JamC and KS due to the docking domains is the main contributor for higher production of **1** *in vitro*.

Evaluation of Site-Directed Mutagenesis of JamC to Improve JamC-PKS Interactions

In addition to docking domains, we also wanted to identify a less-intensive engineering strategy to improve JamC-PKS communication. Mutating JamC without perturbation to the large megasynthase would make this strategy more easily adaptable to different systems. From the well-studied DEBS system, it has been shown that direct ACP-KS protein-protein interactions during translocation are selective, and key residues within helix I of ACP have been identified that contribute to chain translocation specificity (Kapur et al., 2012; Klaus et al., 2016). Inspired by the previous successful studies, we identified the corresponding residue in JamC (E32) that may play an important role in ACP-KS interactions through sequence alignments and structural modeling (Figure S7). To mimic the native upstream ACP, we chose the mutations E32T for

LipPKS1* and E32H for DEBSM6* based on alignments to the respective ACPs found upstream in the native systems (Figure S7). These two JamC mutants were cloned, overexpressed, and purified from BAP1 with a similar yield to the wild-type protein (Figure S1). *In vitro* product formation assays showed that the formation of **1** increased approximately 7-fold with LipPKS1* (Figure 2B) and 2-fold with DEBSM6* (Figure 2C). These fold increases demonstrated the effectiveness of this strategy in improving the production of alkyne-tagged polyketides *in vitro*, most likely due to an improved JamC communication with modular PKSs.

Perturbation of JamB Activity by JamC Engineering

In vitro biochemical assays demonstrated the success of protein engineering in improving the recognition of JamC by PKSs to promote the translocation of the alkynyl starter unit. However, the potential impact of JamC modification on the activity of JamB, the desaturase/acetylenase that functions on a JamC-tethered substrate to form a terminal alkyne, is unclear. As it is difficult to reconstitute and quantify the activity of the membrane-bound JamB *in vitro*, we then tried to implement the biosynthetic machinery of alkyne-tagged polyketides in *E. coli* to assess the possible impact. In addition, the titers of relevant products were also quantified in *E. coli* to probe the effectiveness of two engineering strategies to improve JamC-PKS interactions *in vivo*. Combinations of JamA, B, C, PKSs, and their variants were expressed in an *E. coli* BAP1 strain under a T7 promoter to obtain various engineered strains. A single mutation in JamB (M5T) identified in previous work, presumably with an improved interaction with the electron donor, was used in all strains to increase the alkyne titer in *E. coli* (Zhu et al., 2016). All strains were grown with 5-hexenoic acid feeding, followed by extraction and quantification of 3-hydroxy-7-octenoic acid (**2**) and 3-hydroxy-7-octynoic acid production (**1**), by fitting to a standard curve of synthesized standards generated through liquid chromatography-high-resolution mass spectrometric analysis (Scheme S1, Figures S3, S4, S8, and S9). The product **2** was expected to be a side product due to the activities of JamA, C, and PKS without the action of JamB (Figure 3A). Other possible products were also analyzed, as it is conceivable that the PKSs accept different fatty acyl starter units *in vivo* via JamC or other acyl carriers (Figure S10).

An initial investigation of the titer of compound **1** produced by the co-expression of JamA, B, C, and LipPKS1*/DEBSM6* demonstrated that DEBSM6* produced compound **1** (0.014 mg/L) significantly less than LipPKS1* (0.071 mg/L). Much higher amounts of products other than **1** and **2** with a longer acyl chain were generated by DEBSM6* *in vivo* (Figure S10), consistent with the native acyl chain length accepted by LipPKS1*/DEBSM6* (C4 versus C13). We concluded that DEBSM6* would not be an effective *in vivo* model system to probe the activity of JamB due to complicated product profiles and thus limited the *in vivo* study to LipPKS1*.

The products **1** and **2** were produced by LipPKS1* in an approximately 1:5 ratio, and this efficiency was set to be a relative JamB activity of 100% (Figure 3B). This product ratio was dropped ~4-fold when either docking pair was used, suggesting that the fusion of a docking domain to JamC affected its recognition by JamB (Figure 3B). In contrast, the E32T point mutation of JamC had minimal effect on the product ratio while increasing the titer of **1** ~6-fold to 0.42 mg/L, consistent with previous observations that the helix I of ACP did not play an important role in interacting with JamB (Su et al., 2018; Zhu et al., 2016). We next probed the combined product titer of alkyne **1** and alkene **2** to assess the effectiveness of the two engineering strategies in their ability to improve JamC-LipPKS1* interactions *in vivo* (Figure 3C). Consistent with the trends observed *in vitro*, the combined titer improved more than 10- and 20-fold using docking domains ${}_{C}dd^{CurK}/{}_{N}dd^{CurL}$ and ${}_{C}dd^{JamK}/{}_{N}dd^{JamL}$, respectively, and ~10-fold using JamC (E32T), demonstrating the success of either strategy in improving JamC-PKS interactions *in vivo* (Figure 3C).

Finally, we probed the possible synergistic effects of the two engineering strategies in improving the alkyne-tagged polyketide biosynthesis *in vivo*. We observed additive effects when using docking domains and the JamC point mutation in improving JamC- LipPKS1* interactions. The combined titer of **1** and **2** roughly equaled the sum of that when either engineering strategy was used. The maximum amount of product obtained was ~16 mg/L from JamC(E32T)-${}_{C}dd^{JamK}/{}_{N}dd^{JamL}$-LipPKS1*, an approximately 39-fold increase from unmodified JamC/LipPKS1* (Figure 3C). However, due to the expected disruption of JamB activity when the docking domain is fused to JamC, the absolute titer of the alkyne product **1** was not increased when using both engineering strategies compared with the JamC mutagenesis alone (Figure 3B). These results further highlight the importance of JamB efficiency in *de novo* alkyne synthesis, which remains to be a limiting step in the production of alkyne-tagged polyketides.

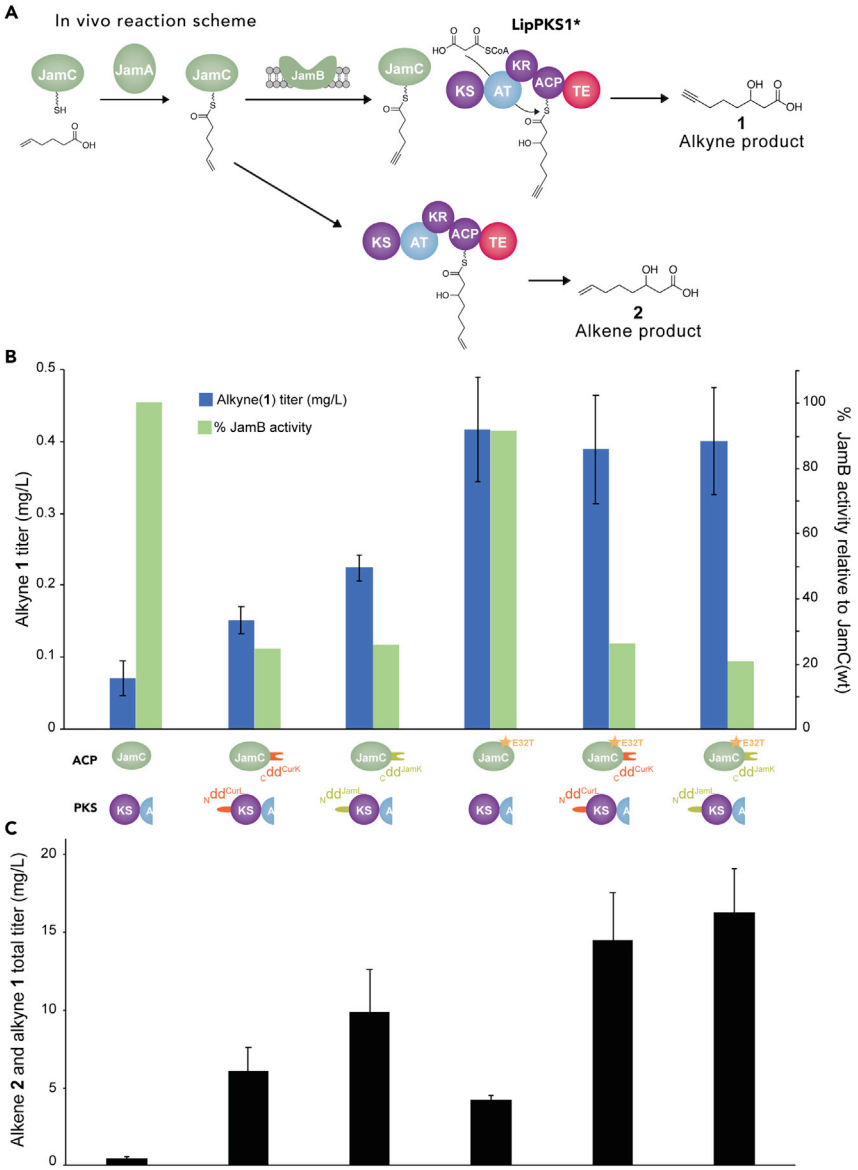

Figure 3. *In Vivo* Assessment of Alkyne-Tagged Polyketide Biosynthesis Using LipPKS1*

(A) Overview scheme of *in vivo* reactions between JamABC and LipPKS1* to produce 3-hydroxy-7-octynoic acid (**1**) and 3-hydroxy-7-octenoic acid (**2**).

(B) Quantification of alkyne product titers resulting from the engineered JamC and LipPKS1*. Alkyne **1** product titers are shown in blue (left y axis), and the relative JamB activities are shown in green (right y axis).

(C) Quantification of total product titers resulting from the engineered JamC and LipPKS1*. LipPKS1* cartoon is truncated for clarity. All titers shown have subtracted background from a control strain lacking JamC to better reflect the interaction between JamC and LipPKS1*. All error bars represent SEM for n ≥ 3 biological replicates.

Limitations of the Study

Although the current results demonstrate a great potential of *de novo* biosynthesizing alkyne-tagged polyketides by engineering both the alkyne biosynthetic machinery and modular type I PKSs, the strategy is limited to incorporate an alkynyl starter unit, which needs to be tolerated by PKSs. It is expected to work well with PKSs with a native starter unit resembling the alkyne-containing acyl group presented by the alkyne biosynthetic machinery, such as in the case of LipPKS1, but may not work with PKSs recognizing very different starter units, such as in the case of DEBSM6. This is particularly exemplified by the *in vivo* results of DEBSM6, in which a complex metabolic background significantly decreased the efficiency of alkyne-tagged polyketide biosynthesis by these PKSs.

Conclusion

We have successfully demonstrated that carrier protein-dependent alkyne biosynthetic machinery can work as a *trans* loading system for truncated Type I PKSs to produce alkyne-tagged polyketides both *in vitro* and *in vivo*. Two protein engineering strategies were explored to improve the interaction between the carrier protein within the alkyne biosynthetic machinery (JamC) and modular PKSs. This included the employment of PKS docking domains and site-directed mutagenesis of JamC to increase acyl chain translocation specificity. Both strategies were shown to be successful, leading to enhanced recognition of JamC by modular PKSs and thus improved alkyne-tagged polyketide production. In addition, the effects of both engineering strategies to improve protein-protein interactions were additive, leading to an ~39-fold increase in the polyketide production by an engineered LipPKS1 in *E. coli*. It is also notable that the installation of a docking domain on JamC, but not the site-directed mutagenesis, disrupted its recognition by JamB in alkyne-tagged polyketide production. Furthermore, the native acyl group specificity of modular PKSs was suggested to be important for alkyne-tagged polyketide production, in particular *in vivo* where competing acyl groups were present. In summary, this work has shown the first examples of *de novo* biosynthesis of alkyne-tagged polyketides by modular type I PKSs through starter unit engineering and further provided engineering guidelines and strategies that are expected to be applicable to other modular PKSs to produce targeted alkyne-tagged metabolites for drug discovery and chemical biology studies.

METHODS

All methods can be found in the accompanying Transparent Methods supplemental file.

SUPPLEMENTAL INFORMATION

Supplemental Information can be found online at https://doi.org/10.1016/j.isci.2020.100938.

ACKNOWLEDGMENTS

Financial support was provided to W.Z. from the NIH (DP2AT009148), Alfred P. Sloan Foundation, and the Chan Zuckerberg Biohub Investigator Program. The authors thank the Joint Bioenergy Institute and the Keasling lab for the generous gift of plasmids containing LipPKS1 and DEBSM6 constructs.

AUTHOR CONTRIBUTIONS

Conceptualization, W.B.P. and W.Z.; Methodology, W.B.P. and W.Z.; Investigation, W.B.P. and N.P.; Writing – Original Draft, W.B.P. and W.Z; Writing – Review & Editing, W.B.P. and W.Z.; Funding Acquisition, W.Z.; Resources, W.Z.; Supervision, W.B.P. and W.Z.

DECLARATIONS OF INTERESTS

W.Z. acted as a guest editor for this special issue of iScience. W.Z took no part in handling of this manuscript.

Received: November 27, 2019
Revised: January 21, 2020
Accepted: February 20, 2020
Published: March 27, 2020

REFERENCES

Awakawa, T., Fujioka, T., Zhang, L.H., Hoshino, S., Hu, Z.J., Hashimoto, J., Kozone, I., Ikeda, H., Shin-Ya, K., Liu, W., et al. (2018). Reprogramming of the antimycin NRPS-PKS assembly lines inspired by gene evolution. Nat. Commun. *9*, 3534.

Barajas, J.F., Blake-Hedges, J.M., Bailey, C.B., Curran, S., and Keasling, J.D. (2017). Engineered polyketides: Synergy between protein and host level engineering. Synth. Syst. Biotechnol. *2*, 147–166.

Bihlmaier, C., Welle, E., Hofmann, C., Welzel, K., Vente, A., Breitling, E., Muller, M., Glaser, S., and Bechthold, A. (2006). Biosynthetic gene cluster for the polyenoyltetramic acid alpha-lipomycin. Antimicrob. Agents Chemother. *50*, 2113–2121.

Chemler, J.A., Tripathi, A., Hansen, D.A., O'Neil-Johnson, M., Williams, R.B., Starks, C., Park, S.R., and Sherman, D.H. (2015). Evolution of efficient modular polyketide synthases by homologous recombination. J. Am. Chem. Soc. *137*, 10603–10609.

Cottens, S., Kallena, J., Schuler, W., and Sedrani, R. (2019). Derivation of rapamycin: adventures in natural product chemistry. Chimia *73*, 581–590.

DeGuire, S.M., Earl, D.C., Du, Y., Crews, B.A., Jacobs, A.T., Ustione, A., Daniel, C., Chong, K.M., Marnett, L.J., Piston, D.W., et al. (2015). Fluorescent probes of the apoptolidins and their utility in cellular localization studies. Angew. Chem. Int. Ed. *54*, 961–964.

Edwards, D.J., Marquez, B.L., Nogle, L.M., McPhail, K., Goeger, D.E., Roberts, M.A., and Gerwick, W.H. (2004). Structure and biosynthesis of the jamaicamides, new mixed polyketide-peptide neurotoxins from the marine cyanobacterium Lyngbya majuscula. Chem. Biol. *11*, 817–833.

Fritsche, K., van den Berg, M., de Boer, W., van Beek, T.A., Raaijmakers, J.M., van Veen, J.A., and Leveau, J.H.J. (2014). Biosynthetic genes and activity spectrum of antifungal polyynes from Collimonas fungivorans Ter331. Environ. Microbiol. *16*, 1334–1345.

Gokhale, R.S., Tsuji, S.Y., Cane, D.E., and Khosla, C. (1999). Dissecting and exploiting intermodular communication in polyketide synthases. Science *284*, 482–485.

Haritos, V.S., Horne, I., Damcevski, K., Glover, K., Gibb, N., Okada, S., and Hamberg, M. (2012). The convergent evolution of defensive polyacetylenic fatty acid biosynthesis genes in soldier beetles. Nat. Commun. *3*, 1150.

Harvey, C.J.B., Puglisi, J.D., Pande, V.S., Cane, D.E., and Khosla, C. (2012). Precursor directed biosynthesis of an orthogonally functional erythromycin analogue: selectivity in the ribosome macrolide binding pocket. J. Am. Chem. Soc. *134*, 12259–12265.

Hertweck, C. (2009). The biosynthetic logic of polyketide diversity. Angew. Chem. Int. Ed. *48*, 4688–4716.

Hughes, A.J., Tibby, M.R., Wagner, D.T., Brantley, J.N., and Keatinge-Clay, A.T. (2014). Investigating the reactivities of a polyketide synthase module through fluorescent click chemistry. ChemComm *50*, 5276–5278.

Jelic, D., and Antolovic, R. (2016). From erythromycin to azithromycin and new potential ribosome-binding antimicrobials. Antibiotics *5*, 29.

Jenke-Kodama, H., and Dittmann, E. (2009). Bioinformatic perspectives on NRPS/PKS megasynthases: Advances and challenges. Nat. Prod. Rep. *26*, 874–883.

Kalkreuter, E., CroweTipton, J.M., Lowell, A.N., Sherman, D.H., and Williams, G.J. (2019a). Engineering the substrate specificity of a modular polyketide synthase for installation of consecutive non-natural extender units. J. Am. Chem. Soc. *141*, 1961–1969.

Kalkreuter, E., Keeler, A.M., Malico, A.A., Bingham, K.S., Gayen, A.K., and Williams, G.J. (2019b). Development of a genetically encoded biosensor for detection of polyketide synthase extender units in Escherichia coli. ACS Synth. Biol. *8*, 1391–1400.

Kalkreuter, E., and Williams, G.J. (2018). Engineering enzymatic assembly lines for the production of new antimicrobials. Curr. Opin. Microbiol. *45*, 140–148.

Kapur, S., Lowry, B., Yuzawa, S., Kenthirapalan, S., Chen, A.Y., Cane, D.E., and Khosla, C. (2012). Reprogramming a module of the 6-deoxyerythronolide B synthase for iterative chain elongation. Proc. Natl. Acad. Sci. U S A *109*, 4110–4115.

Keatinge-Clay, A.T. (2012). The structures of type I polyketide synthases. Nat. Prod. Rep. *29*, 1050–1073.

Khosla, C., Herschlag, D., Cane, D.E., and Walsh, C.T. (2014). Assembly line polyketide synthases: mechanistic insights and unsolved problems. Biochemistry *53*, 2875–2883.

Klaus, M., and Grininger, M. (2018). Engineering strategies for rational polyketide synthase design. Nat. Prod. Rep. *35*, 1070–1081.

Klaus, M., Ostrowski, M.P., Austerjost, J., Robbins, T., Lowry, B., Cane, D.E., and Khosla, C. (2016). Protein-protein interactions, not substrate recognition, dominate the turnover of chimeric assembly line polyketide synthases. J. Biol. Chem. *291*, 16404–16415.

Koryakina, I., Kasey, C., McArthur, J.B., Lowell, A.N., Chemler, J.A., Li, S., Hansen, D.A., Sherman, D.H., and Williams, G.J. (2017). Inversion of extender unit selectivity in the erythromycin polyketide synthase by acyltransferase domain engineering. ACS Chem. Biol. *12*, 114–123.

Ladner, C.C., and Williams, G.J. (2016). Harnessing natural product assembly lines: structure, promiscuity, and engineering. J. Ind. Microbiol. Biotechnol. *43*, 371–387.

Lee, M., Lenman, M., Banas, A., Bafor, M., Singh, S., Schweizer, M., Nilsson, R., Liljenberg, C., Dahlqvist, A., Gummeson, P.O., et al. (1998). Identification of non-heme diiron proteins that catalyze triple bond and epoxy group formation. Science *280*, 915–918.

Marchand, J.A., Neugebauer, M.E., Ing, M.C., Lin, C.I., Pelton, J.G., and Chang, M.C.Y. (2019). Discovery of a pathway for terminal-alkyne amino acid biosynthesis. Nature *567*, 420–424.

McPhail, K.L., Correa, J., Linington, R.G., Gonzalez, J., Ortega-Barria, E., Capson, T.L., and Gerwick, W.H. (2007). Antimalarial linear lipopeptides from a Panamanian strain of the marine cyanobacterium Lyngbya majuscula. J. Nat. Prod. *70*, 984–988.

Minto, R.E., and Blacklock, B.J. (2008). Biosynthesis and function of polyacetylenes and allied natural products. Prog. Lipid Res. *47*, 233–306.

Mohammadi-Ostad-Kalayeh, S., Stahl, F., Scheper, T., Kock, K., Herrmann, C., Batista, F.A.H., Borges, J.C., Sasse, F., Eichner, S., Ongouta, J., et al. (2018). Heat shock proteins revisited: using a mutasynthetically generated reblastatin library to compare the inhibition of human and leishmania Hsp90s. ChemBioChem *19*, 562–574.

Moss, N.A., Seiler, G., Leao, T.F., Castro-Falcon, G., Gerwick, L., Hughes, C.C., and Gerwick, W.H. (2019). Nature's combinatorial biosynthesis produces vatiamides A-F. Angew. Chem. Int. Ed. *58*, 9027–9031.

Moss, S.J., Stanley-Smith, A.E., Schell, U., Coates, N.J., Foster, T.A., Gaisser, S., Gregory, M.A., Martin, C.J., Nur-e-Alam, M., Piraee, M., et al. (2013). Novel FK506 and FK520 analogues via mutasynthesis: mutasynthon scope and product characteristics. MedChemComm *4*, 324–331.

Musiol-Kroll, E.M., Zubeil, F., Schafhauser, T., Hartner, T., Kulik, A., McArthur, J., Koryakina, I., Wohlleben, W., Grond, S., Williams, G.J., et al. (2017). Polyketide bioderivatization using the promiscuous acyltransferase KirCII. ACS Synth. Biol. *6*, 421–427.

Pfeifer, B.A., Admiraal, S.J., Gramajo, H., Cane, D.E., and Khosla, C. (2001). Biosynthesis of complex polyketides in a metabolically engineered strain of E. coli. Science *291*, 1790–1792.

Prescher, J.A., and Bertozzi, C.R. (2005). Chemistry in living systems. Nat. Chem. Biol. *1*, 13–21.

Ranganathan, A., Timoney, M., Bycroft, M., Cortes, J., Thomas, I.P., Wilkinson, B., Kellenberger, L., Hanefeld, U., Galloway, I.S., Staunton, J., et al. (1999). Knowledge-based design of bimodular and trimodular polyketide synthases based on domain and module swaps: a route to simple statin analogues. Chem. Biol. *6*, 731–741.

Rawlings, B.J. (2001). Type I polyketide biosynthesis in bacteria (Part A). Nat. Prod. Rep. *18*, 190–227.

Riva, E., Wilkening, I., Gazzola, S., Li, W.M.A., Smith, L., Leadlay, P.F., and Tosin, M. (2014). Chemical probes for the functionalization of polyketide intermediates. Angew. Chem. Int. Ed. *53*, 11944–11949.

Ross, C., Scherlach, K., Kloss, F., and Hertweck, C. (2014). The molecular basis of conjugated polyyne biosynthesis in phytopathogenic bacteria. Angew. Chem. Int. Ed. *53*, 7794–7798.

Seidel, E.R., Miao, Y.P., Porterfield, L., Cai, W.L., Zhu, X.J., Kim, S.O.O., Hu, F.H., Bhattarai, S.T.L.N., Min, W., and Zhang, W.J. (2019). Structure-activity-distribution relationship study of anti-cancer antimycin-type depsipeptides. Chem. Commun. *55*, 9379–9382.

Seidel, K., Balakrishnan, A., Alexiou, C., Janko, C., Komoll, R.M., Wang, L.L., Kirschning, A., and Ott, M. (2017). Synthesis of magnetic-nanoparticle/ansamitocin conjugates-inductive heating leads to decreased cell proliferation in vitro and attenuation of tumour growth in vivo. Chem. A Eur. J. *23*, 12326–12337.

Staub, I., and Sieber, S.A. (2008). beta-lactams as selective chemical probes for the in vivo labeling of bacterial enzymes involved in cell wall biosynthesis, antibiotic resistance, and virulence. J. Am. Chem. Soc. *130*, 13400–13409.

Su, M., Zhu, X.J., and Zhang, W.J. (2018). Probing the acyl carrier protein-Enzyme interactions within terminal alkyne biosynthetic machinery. Alche J. *64*, 4255–4262.

Sundermann, U., Bravo-Rodriguez, K., Klopries, S., Kushnir, S., Gomez, H., Sanchez-Garcia, E., and Schulz, F. (2013). Enzyme-directed mutasynthesis: a combined experimental and theoretical approach to substrate recognition of a polyketide synthase. ACS Chem. Biol. *8*, 443–450.

Tang, L., Fu, H., and McDaniel, R. (2000). Formation of functional heterologous complexes using subunits from the picromycin, erythromycin and oleandomycin polyketide synthases. Chem. Biol. *7*, 77–84.

Tsuji, S.Y., Cane, D.E., and Khosla, C. (2001). Selective protein-protein interactions direct channeling of intermediates between polyketide synthase modules. Biochemistry *40*, 2326–2331.

Whicher, J.R., Smaga, S.S., Hansen, D.A., Brown, W.C., Gerwick, W.H., Sherman, D.H., and Smith, J.L. (2013). Cyanobacterial polyketide synthase

docking domains: a tool for engineering natural product biosynthesis. Chem. Biol. *20*, 1340–1351.

Wlodek, A., Kendrew, S.G., Coates, N.J., Hold, A., Pogwizd, J., Rudder, S., Sheehan, L.S., Higginbotham, S.J., Stanley-Smith, A.E., Warneck, T., et al. (2017). Diversity oriented biosynthesis via accelerated evolution of modular gene clusters. Nat. Commun. *8*, 1206.

Yan, Y., Chen, J., Zhang, L., Zheng, Q., Han, Y., Zhang, H., Zhang, D., Awakawa, T., Abe, I., and Liu, W. (2013). Multiplexing of combinatorial chemistry in antimycin biosynthesis: expansion of molecular diversity and utility. Angew. Chem. Int. Ed. *52*, 12308–12312.

Yonemoto, I.T., Li, W., Khullar, A., Reixach, N., and Gerratana, B. (2012). Mutasynthesis of a potent anticancer sibiromycin analogue. ACS Chem. Biol. *7*, 973–977.

Yuzawa, S., Deng, K., Wang, G., Baidoo, E.E., Northen, T.R., Adams, P.D., Katz, L., and Keasling, J.D. (2017). Comprehensive in vitro analysis of acyltransferase domain exchanges in modular polyketide synthases and its application for short-chain ketone production. ACS Synth. Biol. *6*, 139–147.

Zeng, J., Wagner, D.T., Zhang, Z.C., Moretto, L., Addison, J.D., and Keatinge-Clay, A.T. (2016). Portability and structure of the four-helix bundle docking domains of trans-acyltransferase modular polyketide synthases. ACS Chem. Biol. *11*, 2466–2474.

Zhang, W.J., Bolla, M.L., Kahne, D., and Walsh, C.T. (2010). A three enzyme pathway for 2-amino-3-hydroxycyclopent-2-enone formation and incorporation in natural product biosynthesis. J. Am. Chem. Soc. *132*, 6402–6411.

Zhu, X.J., Liu, J., and Zhang, W.J. (2015a). De novo biosynthesis of terminal alkyne-labeled natural products. Nat. Chem. Biol. *11*, 115–120.

Zhu, X.J., Shieh, P., Su, M., Bertozzi, C.R., and Zhang, W.J. (2016). A fluorogenic screening platform enables directed evolution of an alkyne biosynthetic tool. Chem. Commun. *52*, 11239–11242.

Zhu, X.J., Su, M., Manickam, K., and Zhang, W.J. (2015b). Bacterial genome mining of enzymatic tools for alkyne biosynthesis. ACS Chem. Biol. *10*, 2785–2793.

Zhu, X.J., and Zhang, W.J. (2015). Tagging polyketides/non-ribosomal peptides with a clickable functionality and applications. Front. Chem. *3*, 11.

iScience, Volume *23*

Supplemental Information

Engineered Biosynthesis of Alkyne-Tagged Polyketides by Type I PKSs

William B. Porterfield, Nannalin Poenateetai, and Wenjun Zhang

Table of contents

Supplementary Figures

A

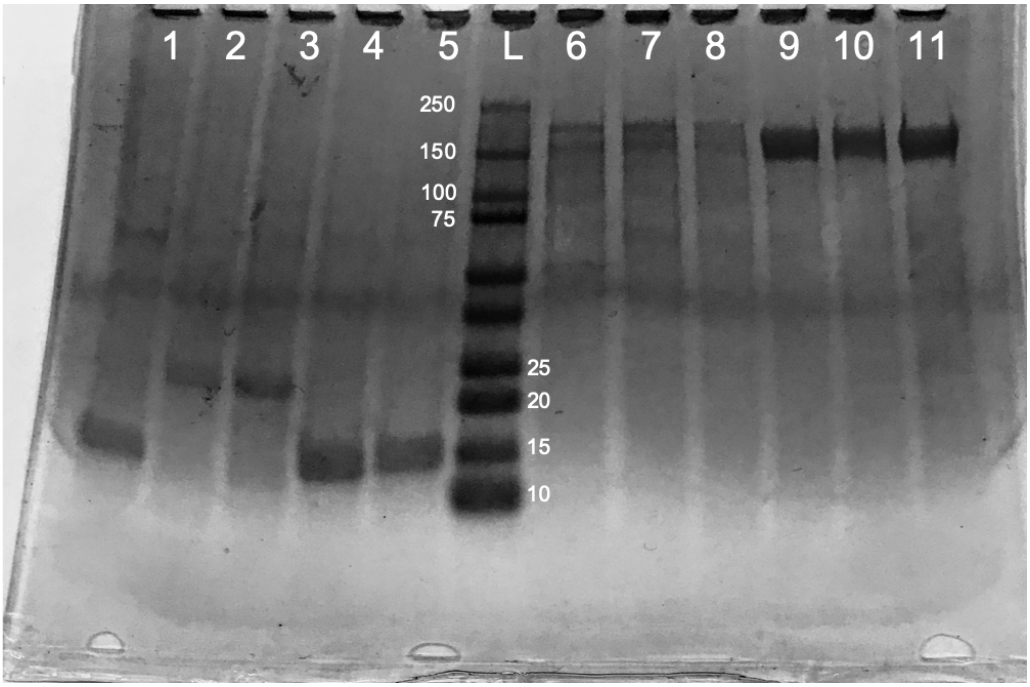

B

number	plasmid	protein	yield (mg/L)	Expected size (kDa)
1	pWP08	JamC	5.0	14.3
2	pWP09	JamC-cdd$_{CurK}$	3.8	20.6
3	pWP11	JamC-cdd$_{JamK}$	7.3	20.5
4	pWP50	JamC(E32T)	3.4	14.3
5	pWP51	JamC(E32H)	4.6	14.3
6	pWP15	LipPKS1*	7.2	192.8
7	pWP17	$_{N}$dd^{CurL}-LipPKS*	3.4	197.0
8	pWP19	$_{N}$dd^{JamL}-LipPKS*	2.6	196.6
9	pSY122	DEBS6M6*	9.2	182.9
10	pWP39	$_{N}$dd^{CurL}-DEBSM6*	3.2	182.9
11	pWP40	$_{N}$dd^{JamL}-DEBSM6*	7.6	182.5

Figure S1. Engineered proteins expressed and purified in this study, related to Figure 2. A. SDS PAGE gel depicting affinity chromatography purified proteins. B. Table giving yields and expected size of proteins shown in the above gel.

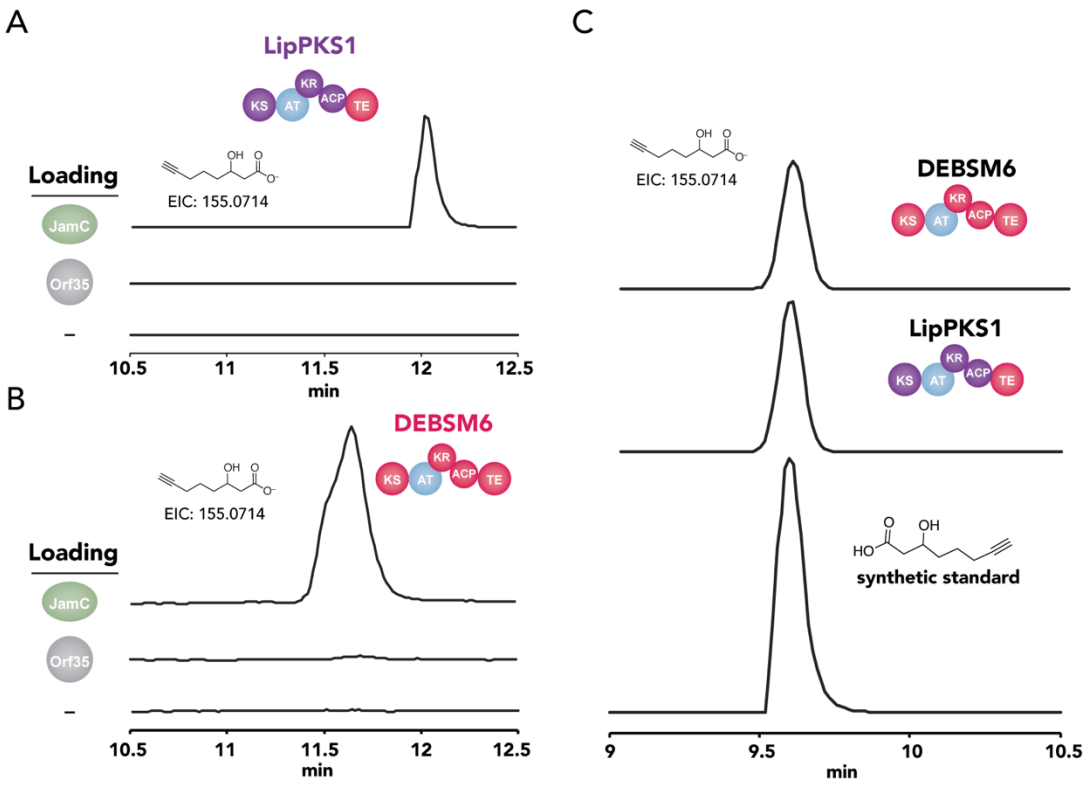

Figure S2. JamA and JamC produced the expected product with LipPKS1* and DEBSM6*, related to Figure 2. **A**. Overview scheme of in vitro reactions between JamA/JamC and model PKSs. **B**. Terminal alkyne product was observed with both PKSs when JamA, JamC, and the PKS are present, but no detectable amounts are observed with the omission of JamC and only trace amounts observed with the inclusion Orf35 in place of JamC. **C.** Comparison of DEBSM6*/LipPKS1* products to a synthetic standard of alkyne product **1**. All solutions in panel C were injected at 15 µl/run with the standard injected at 0.5 ng/mL The experiments in panel A and B were run using an Agilent 6510 Accurate Mass QTOF while experiments in panel C were run on an Agilent 6545 accurate Mass QTOF with a slightly modified gradient (see methods section).

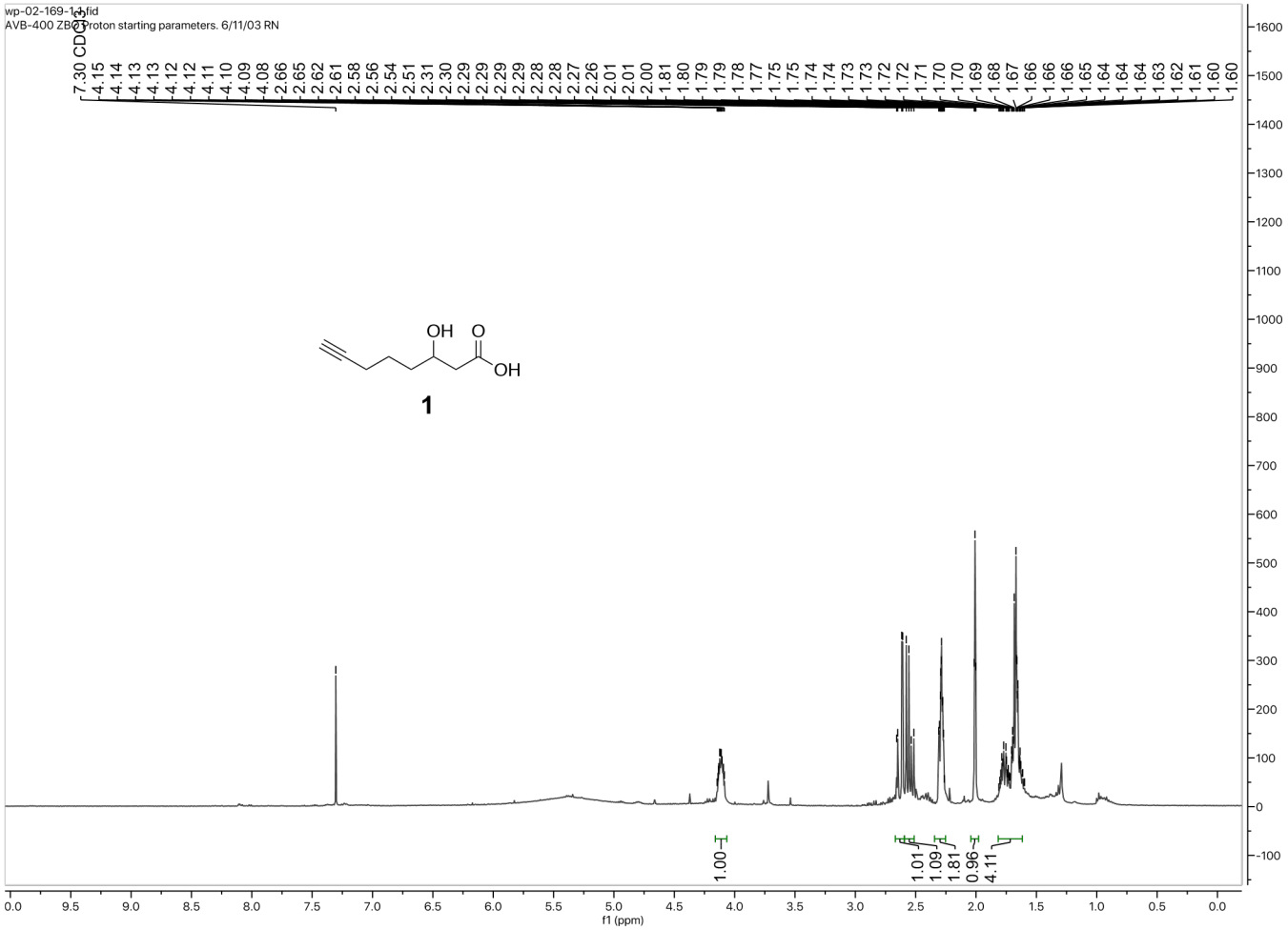

Figure S3. ^{1}H NMR spectra of compound **1** in $CDCl_3$, related to Figure 2 and Figure 3.

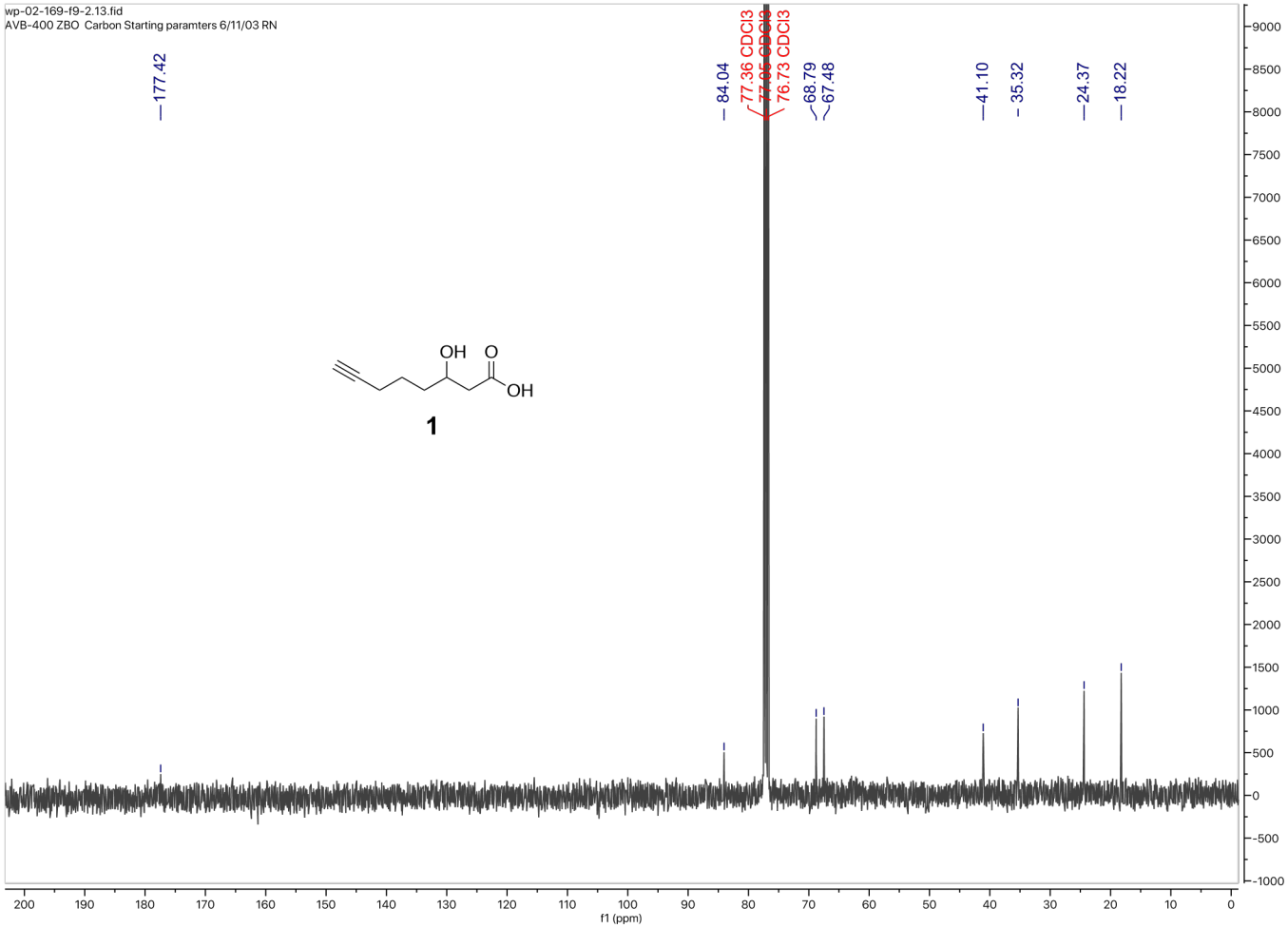

Figure S4. ^{13}C NMR spectra of compound **1** in $CDCl_3$, related to Figure 2 and Figure 3.

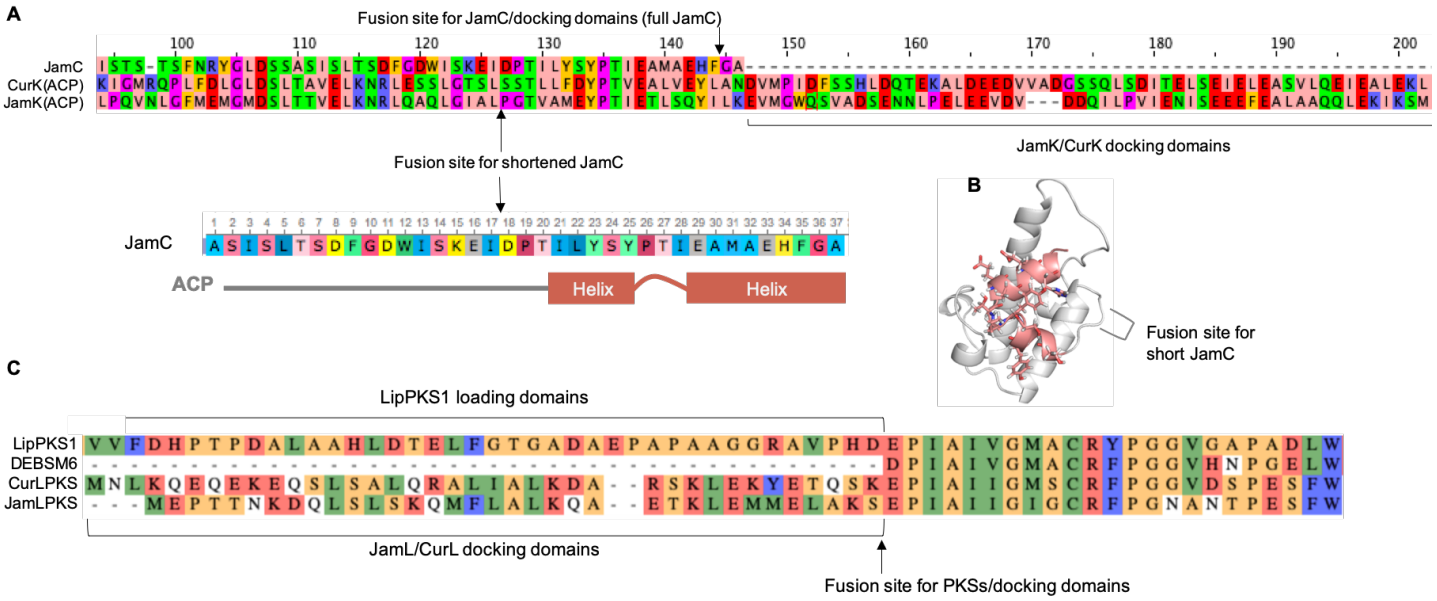

Figure S5. Docking domain alignments, related to Figure 2 and Figure 3. A. Alignments between JamC and $_{C}dd^{CurK}$ and Cdd^{JamK}. Fusion sites for full JamC and also the shortened JamC are shown on the top alignment. Bottom alignment depicts predicted secondary structure of JamC and two helices swapped for longer portions of the docking domains. B. Model of JamC with two C-terminal helices colored salmon and the truncated (short JamC) fusion site highlighted. C. Alignments between LipPKS1, DEBSM6, CurL, and JamL PKSs with the fusion site for the N-terminal docking domains pointed out before the D/EPIAI motif.

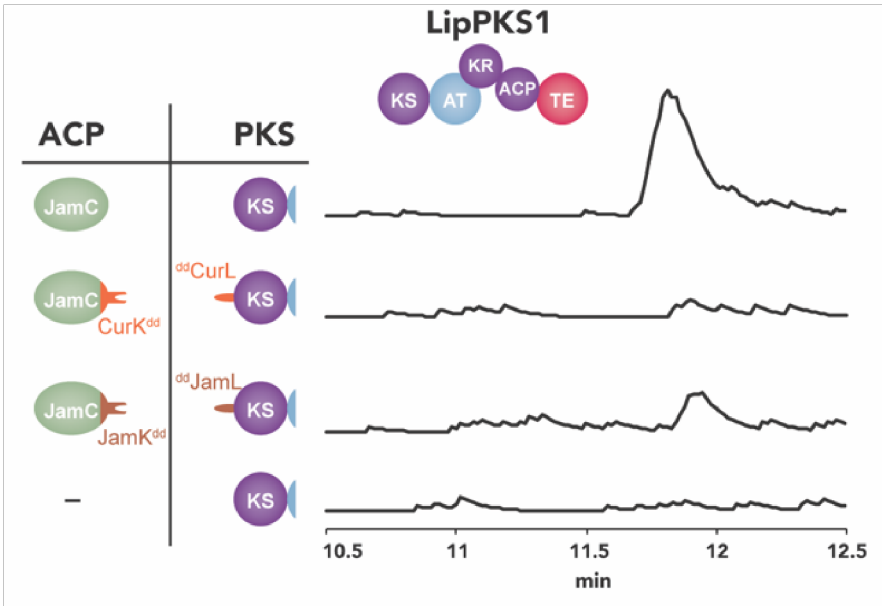

Figure S6. Longer swap of $_{C}dd^{CurK}$ and $_{C}dd^{JamK}$ docking domains do not produce detectable product in vitro, related to Figure 2. Reactions were run at RT for 3h, followed by quenching with cold MeOH. EIC for alkyne product (**1**),155.0714 m/z is shown.

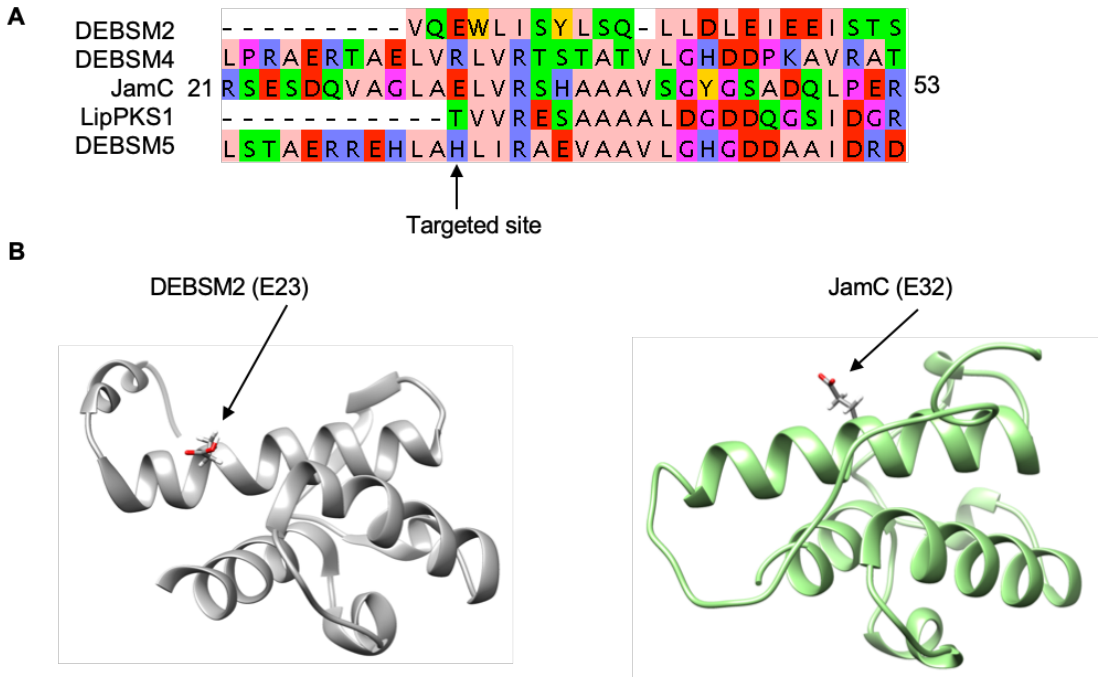

Figure S7. JamC mutagenesis, related to Figure 2 and Figure 3. A. Alignments of JamC compared to DEBSM2-ACP, DEBSM4-ACP, DEBSM5-ACP, and LipPKS1-ACP$_L$. B. Model of JamC residue E32, compared to DEBSM2-ACP residue E23 (PDB: 2JU1). The site directed mutagenesis was inspired by work performed on other modules from the DEBS pathway (Kapur et al., 2012; Klaus et al., 2016). The residue identified was from DEBSM2 and a mutation was made to mimic a residue on the native upstream ACP of DEBSM4. To identify the corresponding residue in JamC alignments of the ACP were performed with the DEBSM2 and DEBSM4 ACPs and JamC. The glutamate at residue 32 of JamC was identified as corresponding to DEBSM2 glutamate at ACP residue 23 through alignments and modelling. Mutating this JamC residue to mimic the native upstream ACP in the LipPKS1 and DEBSM6 required alignments of DEBSM2-ACP to the loading ACP of LipPKS1 and the DEBSM5-ACP, respectively. For the LipPKS1 system the residue was mutated to threonine (E32T), and for DEBSM6 to histidine (E32H).

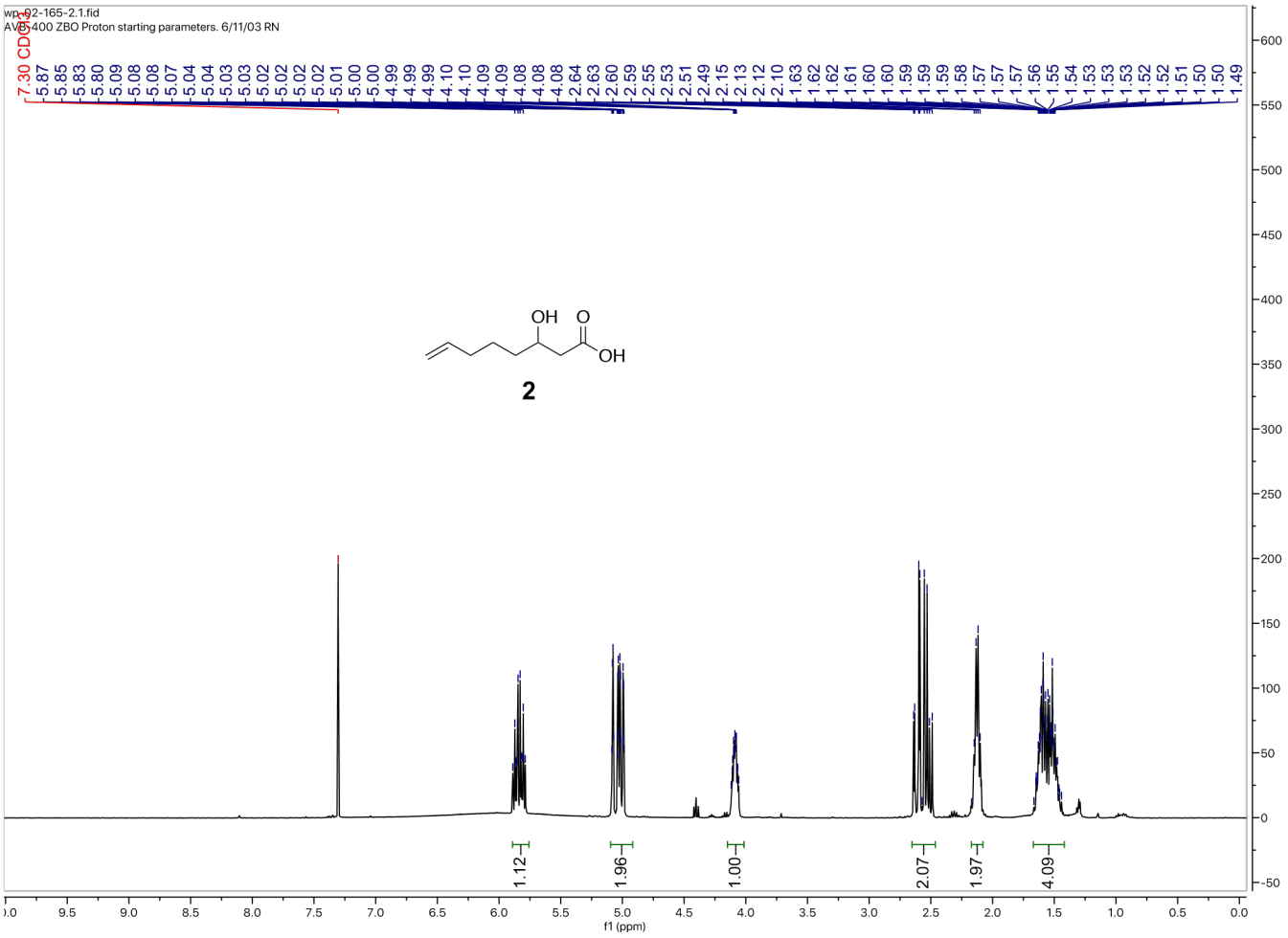

Figure S8. ^{1}H NMR spectra of compound **2** in $CDCl_3$, related to Figure 2 and Figure 3.

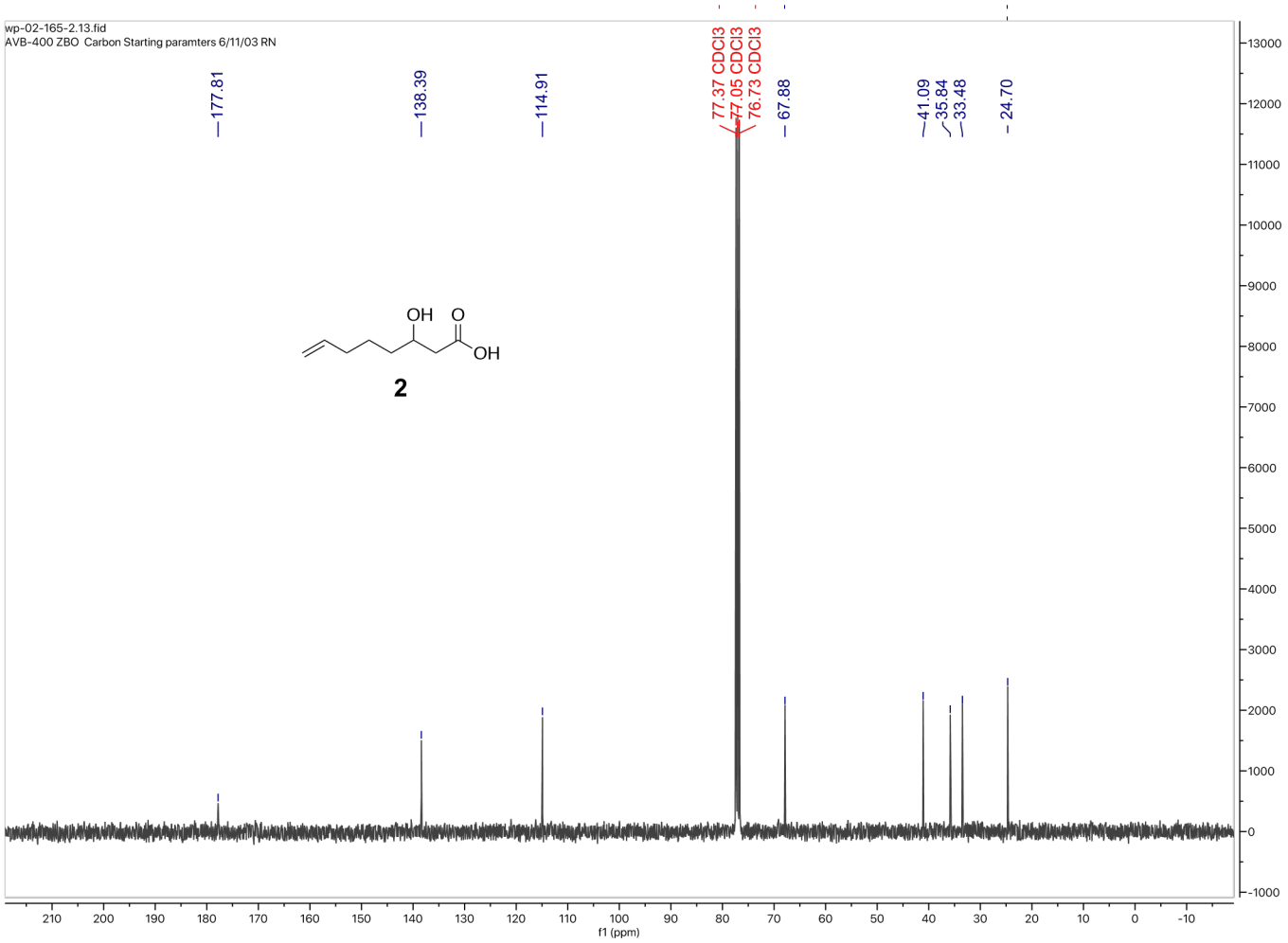

Figure S9: ^{13}C NMR spectra of compound **2** in $CDCl_3$ related to Figure 2 and Figure 3.

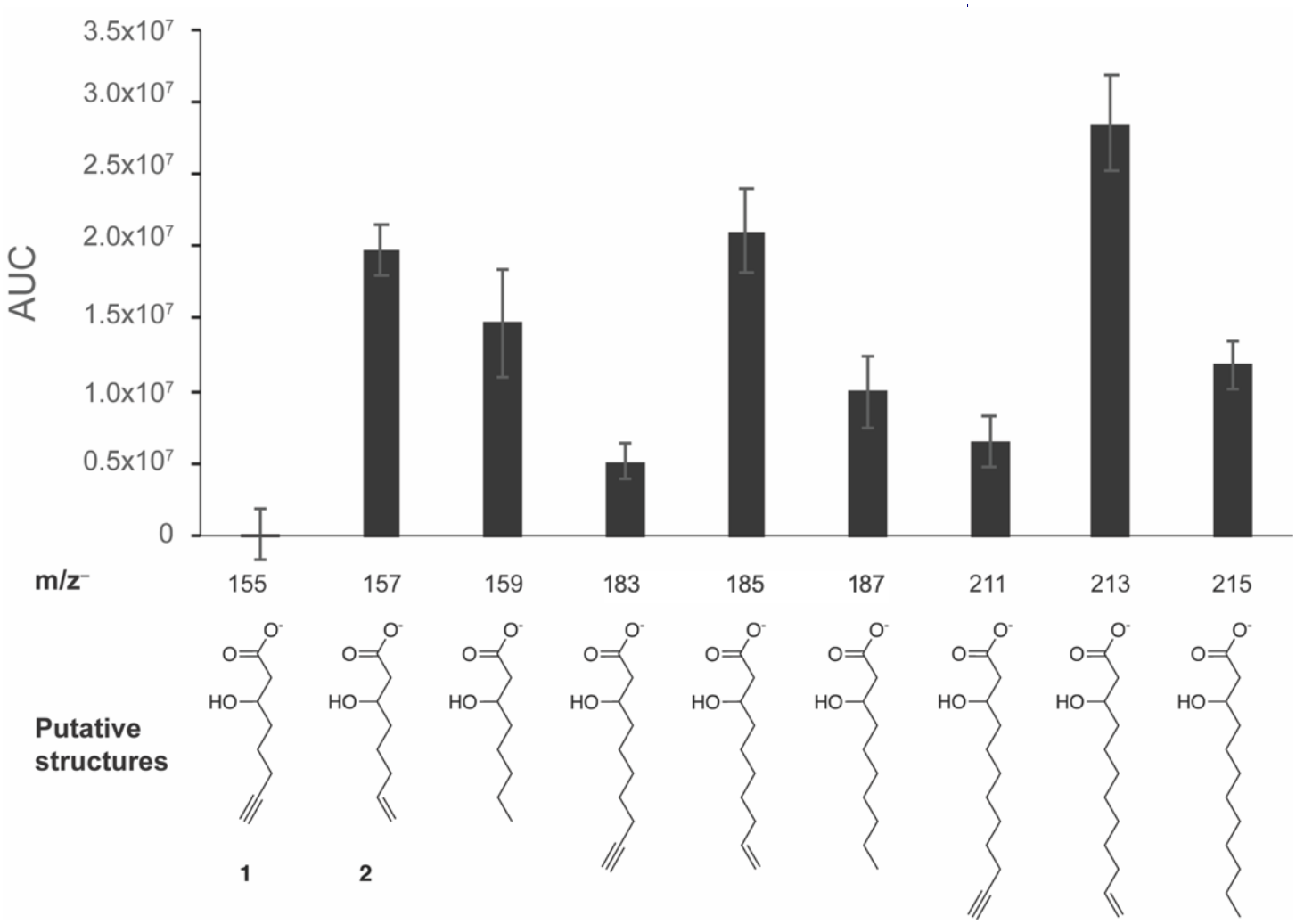

Figure S10. DEBSM6* produced a majority of longer acyl products as compared to compounds **1**, **2,** related to Figure 3. Actual structures for compounds **1** and **2** are shown, while putative structures for other masses are displayed. The y-axis measures Area Under the Curve (AUC) from integrating EIC's for each different compound's mass (see materials and methods for formulas and exact masses). Error bars represent SEM for n ≥ 4 independent experiments.

Transparent methods

General molecular biology methods:

Q5 High-Fidelity DNA polymerase or Phusion High-Fidelity PCR Master Mix (NEB) were used for PCR reactions. Restriction enzymes were purchased from Thermo Scientific. Plasmid construction was performed using the aLICator LIC cloning and expression system (ThermoFisher Scientific), NEB Builder HiFi DNA assembly kit (NEB), or the rapid DNA ligation kit (ThemoFisher Scientific). Constructs for LipPKS1(pSY091) and DEBSM6 (pSY122) were a generous gift from the Keasling lab and the Joint Bioenergy Institute (Yuzawa et al., 2017). Oligonucleotides were ordered from Integrated DNA Technologies and all constructs were confirmed by sequencing through the UC Berkeley DNA sequencing facility. PCRs and digests were run on 0.8%-1% agarose gels and visualized using SYBR safe gel stain (ThermoFisher Scientific). Chemicals and media were obtained from Alfa Aesar, ThermoFisher Scientific, Sigma-Aldrich or other commercial vendors.

Protein expression and purification.

All proteins that were purified contained C- or N-terminal His_6 tags. For protein expression all plasmids were transformed into E. coli BL21 (DE3) Star or BAP1 (for any ACP containing protein). For all proteins except JamA (see below for JamA procedure) the cells were grown at 37 °C in 1 L of LB medium with appropriate concentrations of antibiotics to an OD_{600} of 0.4–0.6. The cells were induced with 0.1-0.25 mM isopropyl-β-D-thiogalactopyranoside (IPTG) for 16 h at 16 °C. The cells were harvested by centrifugation (5,000 x g, 15 min, 4 °C), resuspended in 30 ml of lysis buffer (50 mM HEPES, pH 8.0, 300 mM NaCl, 10 mM imidazole) and lysed by homogenization or sonication (Branson Sonifier 250, power 8, 15 min 30 % duty) on brined ice water. The resultant lysed cells were centrifuged (15,000 x g, 30 min, 4 °C) to remove cell debris. Ni-NTA agarose resin (Qiagen) was added to the supernatant (1-1.5 ml per 1 L of culture), and the solution was nutated at 4 °C for 1 h. The protein resin mixture was loaded onto a gravity flow column, and proteins were eluted with increasing concentrations of imidazole in 50 mM HEPES, pH 8.0, 300 mM NaCl. Purified proteins were concentrated using Amicon Ultra filters, and the buffer was exchanged to remove imidazole with 50 mM HEPES, pH 8.0, 100 mM NaCl. The final proteins were flash-frozen in liquid nitrogen and stored at −80 °C. Protein concentrations were determined by NanoDrop with extinction coefficients calculated using the ExPASy ProtParam tool. Proteins were assessed for correct size and purity by running on mini-PROTEAN precast gels (4-20%, Bio-Rad) at 170 V for 27 min, followed by staining with Bio-Safe Coomassie stain (Bio-Rad). The approximate protein yields are displayed above.

Altered protocol for JamA expression and purification. JamA was transformed into E. coli BL21 (DE3) star cells and grown in autoinduction media (Studier, 2014) for 2 h at 37 °C followed by 16 °C for 12 h. Purification followed the above steps, however 10 % glycerol was included in the buffers during Ni-NTA binding and subsequent purification and buffer exchange steps.

In vitro enzyme assays:

All assays were performed in 100 mM HEPES (pH 8.0) buffer containing 2 mM $MgCl_2$, 20 mM sodium malonate, 2.5 mM TCEP, 1 mM NADPH, 5 mM ATP, 5 mM fatty acid, 2 mM CoA. Malonyl-CoA was generated in vitro with the addition of 10 µM MatB. The following enzymes, when present, were at the following final concentrations: 50 µM ACP, 20 µM PKS, 15 µM JamA, 5 µM Orf35. Reactions were performed at RT for the time indicated (30 min - 3 h). Reactions were quenched with 2 x volume of cold MeOH, followed by centrifugation at 21.1 x g for 3 min. Analysis was performed with LC/HRMS (15 µl injection) with an Agilent Eclipse Plus C18

column (4.6 × 100 mm) and Agilent Technologies 6510 in negative mode. Eluting with a linear gradient of 2–95% MeCN (v/v) over 13 min in H_2O supplemented with 0.1% (v/v) formic acid at a flow rate of 0.5 ml/min. In the experiments shown in Fig. S2C all parameters are the same as the previous sentence besides the reaction run on an Agilent 6545 Accurate Mass QTOF with a linear gradient of 2-98% MeCN (v/v) over 13 min.

In vivo production of 3-hydroxy-7-hexenoic acid and 3-hydroxy-7-hexynoic acid.

BAP1 cells with plasmid pWP34 (pCDFDuet containing JamA and JamB) along with a pETDUET plasmid containing the ACP and PKS were grown in 100 ml of LB medium with 100 µg/ml carbenicillin and 100 µg/ml spectinomycin at 37 °C to an OD_{600} of 0.4–0.6. Subsequently, the cells were centrifuged and resuspended in 25 mL F1 media (60 mM phosphate buffer, pH 7, 30 mM ammonium sulfate, with the following added fresh to a final concentration of 1.25 mM $MgSO_4$, 0.5 % (w/v) glucose, 100 µM $Fe(NH_4)_2(SO_4)_2$) supplemented with 1.25 mL trace metal solution, 10 mL 100 x vitamin solution, 100 µg/ml carbenicillin, 100 µg/ml spectinomycin, 0.5 mM IPTG and 1 mM 5-hexenoic acid. After 72 h of growth at 16 °C, 1 mL of cell culture was added to a 2 mL Eppendorf tube followed by acidification to ~ pH 1 with formic acid (35 µL formic acid). The cell culture was extracted with EtOAc (500 µL x 3). The organic fractions were combined and concentrated using a nitrogen evaporator (Techne). The extract was redissolved in 60 µL MeOH, transferred to mass spec vials and analyzed by HPLC and LC/HRMS (3 µl injection) with an Agilent Eclipse Plus C18 column (4.6 × 100 mm). Eluting with a linear gradient of 2–98% MeCN (v/v) over 13 min in H_2O supplemented with 0.1% (v/v) formic acid at a flow rate of 0.5 ml/min. LC/HRMS analysis was performed on an Agilent Technologies 6545 Accurate Mass QTOF LC/MS in negative mode. Product titers were quantified by calibration to synthetic standards. Integration of product ions from MS/MS fragmentation (Fragmentor set to 100 V and collision energy at 5 V) was performed using the following transitions: 3-hydroxy-7-octenoic acid 157.086 → 59.01 m/z, 3-hydroxy-7-octynoic acid 155.071 → 59.01 m/z. Standard curves were generated for 3-hydroxy-7-octenoic acid (from 50 µg/mL → 0.5 ng/mL, if titer was greater than 50 µg/mL the extract was diluted ten-fold to fit the calibration range) and 3hydroxy-7-octynoic acid (20 µg/mL → 0.5 ng/mL). Data were analyzed and visualized using Agilent MassHunter Q-TOF quantification software and Microsoft Excel. Other compounds besides **1** and **2** with putative structures shown in Figure S10 were confirmed to have the same carboxylic acid MS2 fragment (59.01). The formulas and masses included in other compounds are: $C_8H_{15}O_3^-$–159.1027, $C_{10}H_{15}O_3^-$–183.1027, $C_{10}H_{17}O_3^-$–185.1183,

$C_{10}H_{19}O_3^-$–187.1340, $C_{12}H_{19}O_3^-$–211.1340, $C_{12}H_{21}O_3^-$–213.1496, $C_{12}H_{23}O_3^-$–215.1653. At least three independent replicates were performed, and error bars represent SEM.

Engineered LipPKS1* and DEBSM6*

Previous engineering of the LipPKS1 and DEBSM6 modules swapped the native AT domain for a malonyl-CoA accepting derivative (in our work we used the AT domain derived from the indanomycin module 9 for LipPKS1* and the AT from epothilone module 4 for DEBSM6*) in addition to the thioesterase domain of DEBSM6 fused to the C-terminal end of LipPKS1*, all of these constructs were first reported by Yuzawa *et al.* (Yuzawa et al., 2017) and obtained from the Keasling lab and the Joint Bioenergy Institute.

DEBSM6* was used without further modification in our studies however, LipPKS1 was further modified through removing of the loading domains to create LipPKS1*. The truncation site was chosen based on alignments to other PKSs and the reported site of docking domain fusions (Fig. S5C). Residues 1-646 of LipPKS1 were

removed so that the truncated LipPKS1* begins with the EPIAIV motif. Alignments were performed using Clustal Omega with default settings on the MPI Bioinformatics Toolkit server (Zimmermann et al., 2018).

Docking domain alignments and fusions

Docking domains from the Curacin and Jamaicamide biosynthetic pathways identified by Whicher *et al.* (Whicher et al., 2013). Incorporation of these docking domains necessitated identifying proper fusion sites at the C-terminus of JamC and the N-terminus of the PKSs. To identify the proper sites, we used alignments of the ACPs and PKSs along with structural modeling (Fig. S5A). Two orientations of JamC-docking domain fusions were identified and tested. One with the full JamC ACP with the docking domain appended to the C-terminus and the second with the last 19 residues of JamC were swapped with either CurK or JamK to replace small helices on JamC with those of CurK or JamK in addition to the docking domain (Fig. S5-S6). These $_{C}$dd$^{CurK/JamK}$ constructs were tested with the corresponding $_{N}$dd$^{CurL/JamL}$-LipPKS1* synthase (Fig. S2, S6). The fusion site for the LipPKS1* and DEBSM6* with docking domains were more readily identifiable through alignments thus only one orientation was tested with fusing the docking domain in front of the "D/EPIAI motif" (Fig. S5C).

JamC was modelled using CurA ACP$_{I}$ (PDB: 2LIU) as the parent structure, with the Robetta online server (Song et al., 2013). All alignments were done using Clustal Omega with default settings on the MPI Bioinformatics Toolkit server (Zimmermann et al., 2018).

Site directed mutagenesis identification

The site directed mutagenesis was inspired by work performed on other modules from the DEBS pathway (Kapur et al., 2012; Klaus et al., 2016). The residue identified was from DEBSM2 and a mutation was made to mimic a residue on the native upstream ACP of DEBSM4. To identify the corresponding residue in JamC alignments of the ACP were performed with the DEBSM2 and DEBSM4 ACPs and JamC. The glutamate at residue 32 of JamC was identified as corresponding to DEBSM2 glutamate at ACP residue 23 through alignments and modelling (Fig. S7). Mutating this JamC residue to mimic the native upstream ACP in the LipPKS1 and DEBSM6 required alignments of DEBSM2-ACP to the loading ACP of LipPKS1 and the DEBSM5-ACP, respectively (Fig. S7A). For the LipPKS1 system the residue was mutated to threonine (E32T), and for DEBSM6 to histidine (E32H).

Alignments were performed using Clustal Omega with default settings on the MPI Bioinformatics Toolkit server (Zimmermann et al., 2018). JamC was modelled using CurA ACP$_{I}$ (PDB: 2LIU) as the parent structure, with the Robetta online server (Song et al., 2013).

General synthetic methods:

All reagents were purchased from commercial suppliers and used without further purification. (*R*)-3-Acetyl-4benzyl-2-oxazolidinone (**S3**) was synthesized according to Nickerson *et al. (*Nickerson et al., 2016) and the spectra matched reported literature values (Ager et al., 1996). Reaction progress was monitored by thin-layer chromatography on silica gel 60 plates (aluminum back, EMD Millipore) and visualized by UV light or stained with $KMnO_4$. Compounds were purified by flash column chromatography using Fisher Scientific 230-400 mesh, 60 Å, silica gel. NMR spectra were acquired with a Bruker Biospin spectrometer with a cryoprobe. All spectra were acquired at 298 K. ^{1}H spectra were acquired at 400 MHz, ^{13}C spectra were acquired at 100 MHz. Coupling constants (*J*) are provided in Hz and chemical shifts reported in ppm relative to residual non-deuterated NMR solvent. High resolution mass spectra were collected using an Agilent Technologies 6520 or 6545 Accurate-Mass Q-TOF LC-MS instrument.

Scheme S1: Synthetic route to alkene product **2** (A), and alkyne product **1** (B), related to Figure 2 and Figure 3.

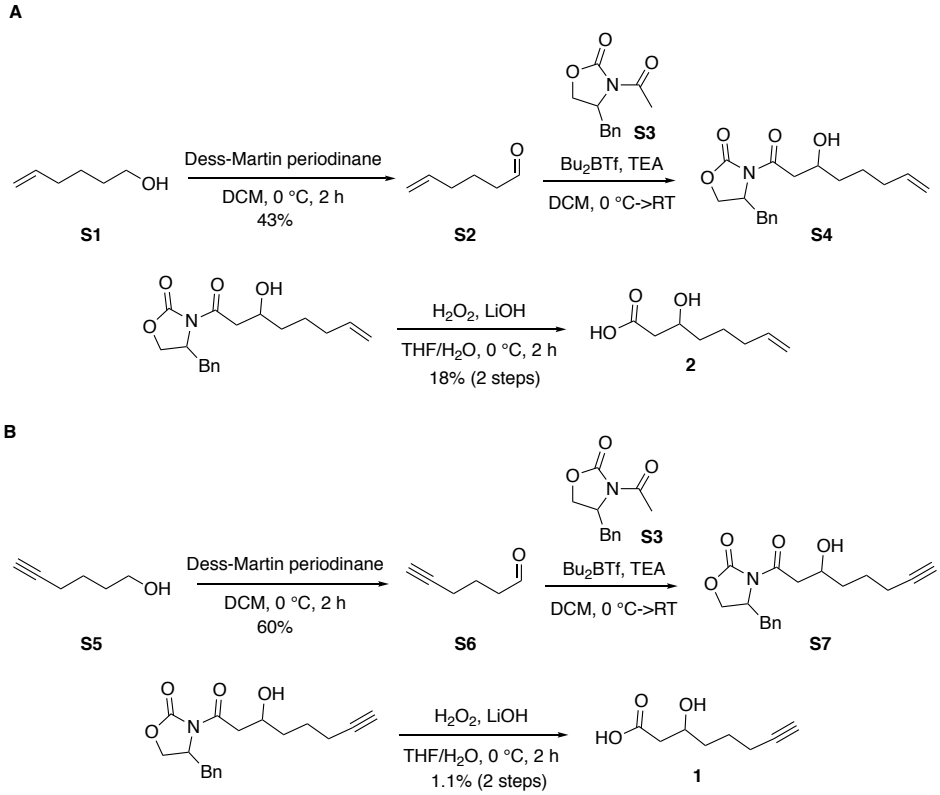

5-hexen-1-al (**S2**):

5-hexen-1-ol (**S1**, 0.72 mL, 6.0 mmol) was added to DCM (60 mL) in a flame-dried round-bottom flask. The solution was cooled to 0 °C and stirred under N_2. Dess-Martin periodinane (3.557 g, 8.386 mmol) was then added to the reaction mixture and stirred for 4.5 h while it warmed to RT. Upon consumption of starting material the reaction was diluted with DCM and washed with saturated sodium bicarbonate (2 x 100 mL). The aqueous layer was extracted with DCM and the organic layers were combined, dried over $MgSO_4$, filtered, and concentrated *in vacuo*. The crude material was purified via flash chromatography (eluting with 9:1 to 7:3 hexanes:ethyl acetate) to provide **S2** as a colorless liquid (0.25 g, 43%). The NMR spectra were consistent with previous reports (Hyugano et al., 2008).

3-hydroxydec-9-enoic acid (**2**):

(*R*)-3-Acetyl-4-benzyl-2-oxazolidinone (**S3**, 0.501 g, 2.29 mmol) was added to a flame-dried round-bottom flask, dissolved in DCM (22 mL), and cooled to 0 °C under N_2. A 1.0 M solution dibutylboron triflate in DCM (2.51 mL, 2.51 mmol) and DIPEA (0.48 mL, 2.7 mmol) were then added to the reaction flask and the mixture was stirred for 30 min at 0 °C followed by cooling to -78 °C. Aldehyde **S2** dissolved in 2 mL DCM was then slowly added to the reaction mixture and stirred for 30 min at -78 °C before warming to RT and stirring an additional 1.5 h. The reaction was monitored by TLC (7:3 hexanes:ethyl acetate) and upon consumption of starting material the reaction was cooled to 0 °C and quenched with 2.5 mL methanol, 1 mL 50 mM phosphate buffer (pH 7.4), and 2

mL of 10% H_2O_2 followed by additional stirring for 1 h. The reaction mixture was diluted with deionized water (20 mL) and extracted with DCM (3 x 20 mL). The organic layers were combined, dried over $MgSO_4$, filtered, and concentrated *in vacuo*. A short silica column was run (eluting with 9:1 to 7:3 hexanes:ethyl acetate) and the relevant fractions were combined and concentrated. The concentrated material was dissolved in 4:1 THF:H_2O (2.2 mL), cooled to 0 °C and 30% H_2O_2 (2.7 mL) was added, followed by slow addition of 1.5 mL sat. LiOH (aq.). The reaction mixture was stirred at 0 °C for 2 h and then quenched with 3 mL sat. Na_2SO_3 and the mixture was extracted with DCM (2 x 10 mL). The organic layer was back-extracted with 10 mL water. The aqueous layers were combined, and the pH was lowered to 1 with 3 M HCl. The aqueous layer was then extracted with ethyl acetate (5 x 20 mL). The organic layers were combined, dried over $MgSO_4$, filtered, and concentrated *in vacuo* to yield an opaque residue. The residue was purified by column chromatography (eluting with 9:1 to 3:2 hexanes:ethyl acetate) to yield **2** as a colorless oil (0.071g, 18%). ^{1}H NMR (400 MHz, $CDCl_3$) d 5.84 (ddt, J = 16.9 Hz, 10.2 Hz, 6.7 Hz, 1H), 5.03 (m, 2H), 4.09 (m, 1H), 2.61 (dd, J = 16.6 Hz, 3.2 Hz, 1H), 2.52 (dd, J = 16.6 Hz, 8.9 Hz, 1H), 2.13 (app q, J = 7.1 Hz, 6.5 Hz, 2H) 1.67-1.42 (m, 4H). ^{13}C NMR (100 MHz, $CDCl_3$) d 177.8, 138.4, 114.9, 67.9, 41.1, 35.8, 33.5, 24.7. HRMS (ES^-) *m/z*: $[M - H]^-$ calcd $C_8H_{13}O_3$ 157.0870, found 157.0875.

5-hexyn-1-al (**S6**):

5-hexyn-1-ol (**S5**, 0.67 mL, 6.1 mmol) was added to DCM (60 mL) in a flame-dried round-bottom flask. The solution was cooled to 0 °C and stirred under N_2. Dess-Martin periodinane (3.630 g, 2.453 mmol) was then added to the reaction mixture and stirred for 4.5 h while it warmed to RT. Upon consumption of starting material the reaction was diluted with DCM and washed with saturated sodium bicarbonate (2 x 100 mL). The aqueous layer was extracted with DCM and the organic layers were combined, dried over $MgSO_4$, filtered, and concentrated *in vacuo*. The crude material was purified via flash chromatography (eluting with 9:1 to 7:3 hexanes:ethyl acetate) to provide **S6** as a colorless liquid (0.35 g, 60%). The NMR spectra were consistent with previous reports (Majmudar et al., 2016).

3-hydroxydec-9-ynoic acid (**1**):

(*R*)-3-Acetyl-4-benzyl-2-oxazolidinone (**S3**, 0.933 g, 4.26 mmol) was added to a flame-dried round-bottom flask, dissolved in DCM (42 mL), and cooled to 0 °C under N_2. A 1.0 M solution dibutylboron triflate in DCM (4.68 mL, 4.68 mmol) and DIPEA (0.89 mL, 5.1 mmol) were then added to the reaction flask and the mixture was stirred for 30 min at 0 °C followed by cooling to -78 °C. Aldehyde **S6** dissolved in 2 mL DCM was then slowly added to the reaction mixture and stirred for 30 min at -78 °C before warming to RT and stirring an additional 1.5 h. The reaction was monitored by TLC (7:3 hexanes:ethyl acetate) and upon consumption of starting material the reaction was cooled to 0 °C and quenched with 5 mL methanol, 2 mL 50 mM phosphate buffer (pH 7.4), and 4 mL of 10% H_2O_2 followed by additional stirring for 1 h. The reaction mixture was diluted with deionized water (40 mL) and extracted with DCM (3 x 40 mL). The organic layers were combined, dried over $MgSO_4$, filtered, and concentrated *in vacuo*. A short silica column was run (eluting with 9:1 to 7:3 hexanes:ethyl acetate) and the relevant fractions were combined and concentrated. The concentrated material was dissolved in 4:1 THF:H_2O (4.0 mL), cooled to 0 °C and 30% H_2O_2 (4.9 mL) was added, followed by slow addition of 2.7 mL sat. LiOH (aq.). The reaction mixture was stirred at 0 °C for 2 h and then quenched with 5 mL sat. Na_2SO_3 and the mixture was extracted with DCM (2 x 20 mL). The organic layer was back-extracted with 20 mL water. The aqueous layers were combined, and the pH was lowered to 1 with 3 M HCl. The aqueous layer was then extracted with ethyl acetate (5 x 30 mL). The organic layers were combined, dried over $MgSO_4$, filtered, and concentrated *in vacuo* to yield an opaque residue. The residue was purified by column chromatography (eluting with a gradient of 5% to 10% methanol in DCM) to yield **1** as a colorless oil (0.0081g, 1.1%). ^{1}H NMR (400 MHz, $CDCl_3$) d

4.11 (m, 1H), 2.63 (dd, J = 16.7 Hz, 3.3 Hz, 1H), 2.55 (dd, J = 16.7 Hz, 8.9 Hz, 1H) 2.29 (m, 2H), 2.01 (t, J = 2.6 Hz, 1H) 1.811.60 (m, 4H). ^{13}C NMR (100 MHz, $CDCl_3$) d 177.4, 84.0, 68.8, 67.5, 41.1, 35.3, 24.4, 18.2. HRMS (ES^-) *m/z*: $[M - H]^-$ calcd $C_8H_{11}O_3$ 155.0714, found 155.0719.

Table S1: Plasmids used in this publication, related to Figure 2 and Figure 3.

Name	description	vector	Use
pWP08	N-term-His WELQ-JamC	pLATE52	JamC overexpression and purification
pWP09	N-term-His WELQ-JamC(full)-CurK(short)	pLATE52	JamC overexpression and purification
pWP10	N-term-His WELQ-JamC(short)-CurK(long)	pLATE52	JamC overexpression and purification
pWP11	N-term-His WELQ-JamC(full)-JamK(short)	pLATE52	JamC overexpression and purification
pWP12	N-term-His WELQ-JamC(short)-JamK(long)	pLATE52	JamC overexpression and purification
pWP15	N-term-His WELQ-LipPKS-AT91	pLATE52	LipPKS1 overexpression and purification
pWP17	N-term-His WELQ-CurL-LipPKS-AT91	pLATE52	LipPKS1 overexpression and purification
pWP19	N-term-His WELQ-JamL-LipPKS-AT91	pLATE52	LipPKS1 overexpression and purification
pWP20	pETDUET-JamC(WT)	pETDUET	Overexpression for in vivo production of terminal alkynes
pWP23	pETDUET-JamC(wt)_LipPKS	pETDUET	Overexpression for in vivo production of terminal alkynes
pWP27	pETDUET-JamC-CurKdd_CurLdd-LipPKS	pETDUET	Overexpression for in vivo production of terminal alkynes
pWP29	pETDUET-JamC-JamKdd_JamLdd-LipPKS	pETDUET	Overexpression for in vivo production of terminal alkynes
pWP30	pETDUET-NL-LipPKS	pETDUET	Overexpression for in vivo production of terminal alkynes
pWP34	pCDFDuet-JamB(M5T)-JamA	pCDFDUET	Overexpression for in vivo production of terminal alkynes
pWP39	pET_CurLdd-DEBSM6	pET	DEBS6 overexpression and purification
pWP40	pET_JamLdd-DEBSM6	pET	DEBS6 overexpression and purification
pWP41	pETDUET-JamC(WT)_DEBS6TE	pETDUET	Overexpression for in vivo production of terminal alkynes
pWP48	pETDUET-DEBS6-TE	pETDUET	Overexpression for in vivo production of terminal alkynes
pWP50	pLATE52-N-His-WELQ-JamC(E32T)	pLATE52	JamC overexpression and purification
pWP51	pLATE52-N-His-WELQ-JamC(E32H)	pLATE52	JamC overexpression and purification
pWP58	pETDUET-JamC(E32T)_LipPKS1	pETDUET	Overexpression for in vivo production of terminal alkynes
pWP59	pETDUET-JamC(E32T)-CurKdd_CurL-LipPKS1	pETDUET	Overexpression for in vivo production of terminal alkynes
pWP65	pETDUET-JamC(E32T)-JamKdd_JamL-LipPKS1	pETDUET	Overexpression for in vivo production of terminal alkynes
pWP73	pCDFDuet-JamB(M5T)	pCDFDUET	Overexpression for in vivo production of terminal alkynes
PSY122	DEBS6-TE	pET	Overexpression and purification of DEBSM6
PXZ23	JamA	pET	Overexpression and purification of JamA

Table S2: Primers used to generate plasmids, related to Figure 2 and Figure 3.

Primer	sequence (5´-->3´)	Used for
PWP24-His-WELQ-JamC-pLATE-fwd	GGTTGGGAATTGCAAATGGAAAACTTAACCGTAGAAACC	JamC cloning into pLATE52 for overexpression
PWP25-JamC-wt-pLATE-Rev	ggagatgggaagtcattaTGCACCAAAGTGCTCTG	JamC docking domain cloning
PWP26-JamC-fu-CurK-sh-Fwd	GCTATGGCAGAGCACTTTGCAAATGATGTGATGCCGAT	JamC docking domain cloning
PWP27-CurK-sh-JamC-fu-Rev	ATCGGCATCACATCATTTGCAAAGTGCTCTGCCATAGC	JamC docking domain cloning
PWP28-CurK-pLATE52-rev	ggagatgggaagtCATTAGATTAACTTCTCCAAAGCTTCGAT	JamC docking domain cloning into pLATE52 for overexpression
PWP29-JamC-sh-CurK-long-Fwd	tggggattggatctcaaaagaaataTCCTCTACCTTATTATTCGACTATCC	JamC docking domain cloning
PWP30-CurK-long-JamC-sh-Rev	GGATAGTCGAATAATAAGGTAGAGGAtatttcttttgagatccaatcccca	JamC docking domain cloning
PWP31-JamC-fu-JamK-sh-Fwd	GCTATGGCAGAGCACTTTCTGAAGGAAGTTATGGGCTG	JamC docking domain cloning
PWP32-JamK-sh-JamC-fu-Rev	CAGCCCATAACTTCCTTCAGAAAGTGCTCTGCCATAGC	JamC docking domain cloning into pLATE52 for overexpression
PWP33-JamK-pLATE52-Rev	ggagatgggaagtCATTACAACATCGACTTGATTTTCTCAA	JamC docking domain cloning into pLATE52 for overexpression
PWP34-JamC-sh-JamK-long-Fwd	tggggattggatctcaaaagaaataCCTGGCACCGTCG	JamC docking domain cloning
PWP35-JamK-long-JamC-sh-Rev	CGACGGTGCCAGGtatttcttttgagatccaatcccca	JamC docking domain cloning
PWP38-pLATE52-LipPKS-KS-fwd	ggttgggaattgCAAgaaccaattgcgatcgtgg	LipPKS1 cloning into pLATE52 for overexpression
PWP39-TE-LipPKS-pLATE52-Rev	ggagatgggaagtCATTAGCTGTTGCCGCCA	LipPKS1 cloning into pLATE52 for overexpression
PWP40-pLATE52-CurL-Fwd	ggttgggaattgCAAATGAACCTTAAGCAAGAGCAG	LipPKS1 docking domain cloning into pLATE52 for overexpression
PWP41-LipPKS-KS-CurL-Rev	ccacgatcgcaattggttcTTTTGATTGAGTCTCATACTTCTCTAACTT	LipPKS1 docking domain cloning
PWP41-CurL-LipPKS-KS-Fwd	AAGTTAGAGAAGTATGAGACTCAATCAAAAgaaccaattgcgatcgtgg	LipPKS1 docking domain cloning
PWP42-pLATE52-JamL-Fwd	ggttgggaattgCAAATGGAACCTACCACGAATAAGG	LipPKS1 docking domain cloning into pLATE52 for overexpression
PWP43-LipPKS-KS-JamL-Rev	ccacgatcgcaattggttcGGATTTAGCCAACTCCATCATC	LipPKS1 docking domain cloning
PWP44-JamL-LipPKS-KS-Fwd	GATGATGGAGTTGGCTAAATCCgaaccaattgcgatcgtgg	LipPKS1 docking domain cloning
PWP48-JamC-all-Fwd	catCCATGGAAAACTTAACCGTAGAAA	JamC cloning into pETDUET
PWP49-JamC-Rev	catAAGCTTCTAtgcaccaaagtgctct	JamC cloning into pETDUET
PWP50-JamC-CurKdd-Rev	catAAGCTTCTAGATTAACTTCTCCAACGCTTCGATTTCTTG	JamC cloning into pETDUET
PWP51-JamC-JamKdd-Rev	catAAGCTTCTACAACATCGACTTGATTTTCT	JamC cloning into pETDUET
PWP52-LipPKS-wt-Fwd	tacCATATGGAACCAATTGCGATCG	LipPKS1 cloning into pETDUET
PWP53-CurLdd-LipPKS-Fwd	tacCATATGAACCTTAAGCAAGAGCA	LipPKS1 cloning into pETDUET
PWP54-JamLdd-LipPKS-Fwd	tacCATATGGAACCTACCACGAATA	LipPKS1 cloning into pETDUET
PWP55-LipPKS-all-REV	catCTCGAGtcaGCTGTTGCCGCC	LipPKS1 cloning into pETDUET
PWP56-pETDUET-LipPKS-Fwd	ttaagtataagaaggagatatacatATGGAACCAATTGCGATCGTGG	LipPKS1 cloning into pETDUET
PWP57-pETDUET-CurLdd-Fwd	ttaagtataagaaggagatatacatATGAACCTTAAGCAAGAGCAGGAAAAAG	CurL cloning into pETDUET
PWP58-pETDUET-JamLdd-Fwd	ttaagtataagaaggagatatacatATGGAACCTACCACGAATAAGGACC	JamLcloning into pETDUET
PWP59-LipPKS-pETDUET(end)-Rev	cagcggtttctttaccagactcgagTCAGCTGTTGCCGCCACC	LipPKS1 cloning into pETDUET
PWP60-pETDUET(2nd MCS)-Fwd	CTCGAGTCTGGTAAAGAAAC	pETDUET MCS2 cloning
PWP61-pETDUET(2nd MCS)-Rev	ATGTATATCTCCTTCTTATACTTAACTAATATACTAAGATGGG	pETDUET MCS2 cloning
PWP74-pCDF-JamB-M5T-Fwd	ctttaataaggagatataccATGTCAATGCCAACCGATGTGAGCAA	JamB(M5T) mutation cloning into pCDFDuet
PWP75-JamB-PCDF-rev	gcaagcttgtcgacctgcagTTAAGCTAACTTCTTAGCTTCG	JamB(M5T) mutation cloning into pCDFDuet
PWP89-pET_Gibson-Rev	ATGTATATCTCCTTCTTAAAGTTAAAC	pET Gibson cloning for overexpression
PWP90-pETGibson-Fwd	GATCCGGCTGCTAACAAAGCC	pET Gibson cloning for overexpression
PWP91-pET-CurLdd-Fwd	ttaactttaagaaggagatatacatATGAACCTTAAGCAAGAG	pET CurL cloning for overexpression
PWP92-CurLdd-DEBS6-Rev	tcgcaatcggatcTTTTGATTGAGTCTCATACTTC	DEBS6 docking domain cloning
PWP93-CurLdd-DEBS6-Fwd	gactcaatcaaaaGATCCGATTGCGATTGTGG	DEBS6 docking domain cloning
PWP94-DEBS6-pET-Rev	ttcgggctttgttagcagccggatcTCAGTGGTGGTGGTGGTG	DEBS6 into pET for overexpression cloning

PWP95-pET-JamLdd-Fwd	ttaactttaagaaggagatatacatATGGAACCTACCACGAATAAG	pET JamL cloning for overexpression
PWP96-JamLdd-DEBS6-Rev	TCGCAATCGGATCGGATTTAGCCAACTCCATC	DEBS6 docking domain cloning
PWP97-JamLdd-DEBS6-Fwd	gttggctaaatccGATCCGATTGCGATTGTGG	DEBS6 docking domain cloning
PWP110_pETDUET-DEBS6_fwd	ttaagtataagaaggagatatacatATGTCTGGTGATAACGGCATG	DEBS6 cloning into pETDUET
PWP111_DEBS6-pETDUET_rev	cagcggtttctttaccagactcgagtcacgaattcccgccac	DEBS6 cloning into pETDUET
PWP144_JamC_E32T_fwd	agatgaggttcagACCtggttgatttcttatc	JamC mutagenesis cloning
PWP145_JamC_E32T_rev	gataagaaatcaaccaGGTctgaacctcatct	JamC mutagenesis cloning
PWP146_JamC_E32H_fwd	AGATGAGGTTCAGCATTGGTTGATTTCTTATC	JamC mutagenesis cloning
PWP147_JamC_E32H_rev	gataagaaatcaaccaATGctgaacctcatct	JamC mutagenesis cloning
PWP158_pETDUET_MCS1_fwd	AAGCTTGCGGCCGCATAAT	pETDUET MCS1 cloning
PWP159_pETDUET_MCS1_rev	GGTATATCTCCTTCTTAAAGTTAAACAAAATTATTTCTAGAGG	pETDUET MCS1 cloning
PWP160_pETDUET_JamC-Fwd	ctttaagaaggagatataccATGGAAAACTTAACCGTAGAAAC	pETDUET JamC cloning
PWP161_pETDUET_JamC-Rev	cattatgcggccgcaagcttCTATGCACCAAAGTGCTC	pETDUET JamC cloning
PWP162_pETDUET_CurKdd-Rev	cattatgcggccgcaagcttCTAGATTAACTTCTCCAACG	pETDUET JamC cloning
PWP163_pETDUET_JamKdd-Rev	cattatgcggccgcaagcttCTACAACATCGACTTGATTTTC	pETDUET JamC cloning
PWP166_QC_JamC_E32T_fwd	cagtagatgaggttcagacctggttgatttcttatctatcacaa	JamC mutagenesis cloning (quick change)
PWP167_QC_JamC_E32T_rev	ttgtgatagataagaaatcaaccaggtctgaacctcatctactg	JamC mutagenesis cloning (quick change)

References

Ager, D.J., Allen, D.R., and Schaad, D.R. (1996). Simple and efficient N-acylation reactions of chiral oxazolidinone auxiliaries. Synthesis-Stuttgart, 1283-&.

Hyugano, T., Liu, S., and Ouchi, A. (2008). Facile Photochemical Transformation of Alkyl Aryl Selenides to the Corresponding Carbonyl Compounds by Molecular Oxygen: Use of Selenides as Masked Carbonyl Groups. J. Org. Chem. 73, 8861-8866.

Kapur, S., Lowry, B., Yuzawa, S., Kenthirapalan, S., Chen, A.Y., Cane, D.E., and Khosla, C. (2012). Reprogramming a module of the 6-deoxyerythronolide B synthase for iterative chain elongation. Proc. Natl. Acad. Sci. U.S.A. 109, 4110-4115.

Klaus, M., Ostrowski, M.P., Austerjost, J., Robbins, T., Lowry, B., Cane, D.E., and Khosla, C. (2016). Protein-Protein Interactions, Not Substrate Recognition, Dominate the Turnover of Chimeric Assembly Line Polyketide Synthases. J. Biol. Chem. 291, 16404-16415.

Majmudar, J.D., Konopko, A.M., Labby, K.J., Tom, C.T.M.B., Crellin, J.E., Prakash, A., and Martin, B.R. (2016). Harnessing Redox Cross-Reactivity To Profile Distinct Cysteine Modifications. J. Am. Chem. Soc. 138, 1852-1859.

Nickerson, L.A., Huynh, V., Balmond, E.I., Cramer, S.P., and Shaw, J.T. (2016). Asymmetric Synthesis of Homocitric Acid Lactone. J. Org. Chem. 81, 11404-11408.

Song, Y.F., DiMaio, F., Wang, R.Y.R., Kim, D., Miles, C., Brunette, T.J., Thompson, J., and Baker, D. (2013). High-Resolution Comparative Modeling with RosettaCM. Structure 21, 1735-1742.

Studier, F.W. (2014). Stable Expression Clones and Auto-Induction for Protein Production in E-coli. Structural Genomics: General Applications 1091, 17-32.

Whicher, J.R., Smaga, S.S., Hansen, D.A., Brown, W.C., Gerwick, W.H., Sherman, D.H., and Smith, J.L. (2013). Cyanobacterial Polyketide Synthase Docking Domains: A Tool for Engineering Natural Product Biosynthesis. Chem. Biol. 20, 1340-1351.

Yuzawa, S., Deng, K., Wang, G., Baidoo, E.E., Northen, T.R., Adams, P.D., Katz, L., and Keasling, J.D. (2017). Comprehensive in Vitro Analysis of Acyltransferase Domain Exchanges in Modular Polyketide Synthases and Its Application for Short-Chain Ketone Production. ACS Synth. Biol. 6, 139-147.

Zimmermann, L., Stephens, A., Nam, S.Z., Rau, D., Kubler, J., Lozajic, M., Gabler, F., Soding, J., Lupas, A.N., and Alva, V. (2018). A Completely Reimplemented MPI Bioinformatics Toolkit with a New HHpred Server at its Core. J. Mol. Biol. 430, 2237-2243.